



Research Article

Long-Term Seismic Monitoring of a Passively-Controlled Steel Building on Performance Assessment under Strong Earthquake

Yunjia Tong ¹, Songtao Xue,^{2,3} Liyu Xie ² and Hesheng Tang²

¹School of Civil and Architectural Engineering, Henan University, Kaifeng 475001, China

²Department of Disaster Mitigation for Structures, Tongji University, Shanghai 200092, China

³Department of Architecture, Tohoku Institute of Technology, Sendai 982-8577, Japan

Correspondence should be addressed to Liyu Xie; liyuxie@tongji.edu.cn

Received 7 November 2022; Revised 12 March 2023; Accepted 17 June 2023; Published 12 October 2023

Academic Editor: Łukasz Jankowski

Copyright © 2023 Yunjia Tong et al. This is an open access article distributed under the Creative Commons Attribution License, which permits unrestricted use, distribution, and reproduction in any medium, provided the original work is properly cited.

Analysis of recorded seismic response of an eight-story passively-controlled steel building located in Sendai is reported in this paper. Vibration monitoring system has been instrumented to test the effectiveness of dampers and actual performance of passively-controlled structures under earthquake since it was constructed in 2003. A data-driven stochastic subspace identification methodology with an alternative strategy to remove spurious modes is developed and implemented to the recorded actual earthquake response to extract dynamic properties of the passively-controlled eight-story steel building from the recorded floor acceleration data. Thus, the inherent damping characteristic of the building is identified under various earthquakes. Moreover, the variation of the estimated natural frequencies, mode shapes, and damping ratios for all the earthquake recordings are illustrated. To further investigate serviceability of the passively-controlled steel building during an earthquake, probabilistic model updating is developed to estimate the model parameters and infer the response of the structure based on the identified modes. Besides, seismic performance assessment of the passively-controlled steel building from the estimated dynamic characteristics and model parameters during service period is also discussed.

1. Introduction

The passive structural control method has been widely used in earthquake engineering since the 1970s to minimize structural vibration because the construction and operation of passive control devices are extremely simple and robust, with no need for actuators, external power supplies, or sensors [1]. As extra passive dampening devices can significantly improve the vibrational performance of structures by absorbing and dissipating much of the input energy that would otherwise be absorbed by the building's lateral load resisting system, the structure's forced vibration, displacement, acceleration, and inelastic deformation are greatly reduced [2].

In the context of civil engineering, passive dampening devices primarily include hysteretic dampers, friction dampers, velocity-dependent dampers (such as viscous fluid dampers and viscoelastic dampers), and tuned mass

dampers, among others [3–6]. They can generally be relied upon to reduce the risks posed by wind and earthquakes as well as to renovate decaying structures. More than 7,000 buildings in Japan have seismic isolators or auxiliary damping mechanisms, according to the Japan Society of Seismic Isolation [7]. Extensive experimental investigations on passively-controlled structural models as well as various passively-controlled devices (full-scale or small-scale) have been performed [8–10]. Design provisions and guidelines have also been developed for the passively-controlled building structures and passively-controlled devices [11]. Nevertheless, it has seldom been possible to test the actual performance of passively-controlled structures by actual earthquakes and the actual performance of the passive devices after deployment during major and catastrophic earthquakes, due to the fact that throughout the shaking table testing, the frame members of the structures remained largely elastic. Thus, it is extremely important to examine

and evaluate realistic earthquake behavior of such structural systems during strong earthquake based on real-time seismic response monitoring.

Capturing and understanding of actual phenomena and the underlying properties are very important and should be supported by the investigation on actual data and related theories [12]. Loh et al. analyzed the recorded seismic response of three structures (one isolated bridge, one mid-isolation building, and one 7-story RC building) during the period of service based on dynamic characteristics estimation, presented the variation of the dynamic characteristics of the buildings, and discussed the seismic assessment of the buildings [13]. Siringoringo and Fujino analyzed strong motion recordings of an asymmetric base-isolated building during the March 11, 2011, Great East Japan (Tohoku) Earthquake [14]. The aforementioned investigations and strong motion observations provide valuable insights into the behavior of passively-controlled buildings.

In general, system identification techniques are employed to the recorded actual earthquake response to extract dynamic properties from the system [15, 16]. Versatile researches have been conducted on the identification of dynamic characteristics of structures using earthquake-induced motion data, which are meaningful for earthquake-resistant design, model validation, and structural health monitoring [17–19]. Among them, subspace identification algorithm had been applied to multiple earthquake records because of simple parameterization for MIMO systems in the past few years. Various versions of subspace algorithms such as CVA, N4SID, MOESP, and IV-4SID have been utilized to estimate the state space model of the systems [20–22]. However, the model order selection is nontrivial and crucial for successfully identifying the inherent damping characteristic of the building. Because the chosen model orders are typically and significantly greater than twice the number of important modes that comprise the majority of the structural response, the “spurious” numerical modes are attributed to the detected modes. Separating the “genuine” modes from “spurious” modes can still be a challenge due to sensor noise and measurement errors [23], even though model order has been determined.

To consistently pick the “genuine” modes, the stabilization diagram, which will be utilized in the following section, is used to distinguish true modes from false ones. The stabilization diagram can depict the relative differences between each mode. As a result, by comparing the dynamic features of these two approaches, true modes can be distinguished from spurious modes. Nevertheless, mathematical mode may pass the stabilization criteria in few special cases. A different approach of constructing the system matrix A is proposed as validation criteria to remove the above mathematical mode [24].

Besides, updating structural model and state is also crucial for structural health monitoring and control, as it is generally concerned with evaluating structural health condition, dynamic responses, and remaining lifetime [25–27]. Bayesian model updating is commonly used to identify structural model for performance evaluation and subsequently reliable assessment of its behavior under future

loads [28–30]. Due to its ability of qualifying different sources of uncertainties, probabilistic model updating procedures are broadly utilized for the preservation of cultural heritage (historic masonry buildings, towers, churches, etc.) [31–33]. At the same time, probabilistic model updating procedures have also been developed for detecting damage and condition assessment of high-rise buildings and long-span bridges instrumented with structural health monitoring systems [34–37].

In general, structural initial model is built according to structural design drawings without considering the construction uncertainties, aging, and degradation, as well as variation. Thus, the initial model cannot accurately represent the actual structural state and behavior. To calibrate the structural model, Bayesian inference framework is exploited to update structural model and to quantify the modeling uncertainties based on the above identified modes from actual monitoring data. Nevertheless, there is a practical difficulty for implementing Bayesian model updating, since limited sensors are available in most cases due to the cost or damage. To cope with this difficulty, model reduction approach is introduced to the Bayesian model updating algorithm considering the available measurements. A Markov chain Monte Carlo algorithm [38] is then used to approximate the probabilistic distributions of the model parameters. Thus, seismic performance assessment and structural response prediction can be conducted.

In this paper, a passively controlled eight-story steel building equipped with energy dissipation devices is investigated under real earthquake. Vibration monitoring apparatuses have been installed on the main structure and on the dampers to evaluate the long-term behavior of the passively controlled structure, which also provide a prospective on the actual performance of passive devices in service. Moreover, knowledge of passively controlled structural demand during strong earthquakes can be accumulated to provide a better understanding of the structural behavior in nonlinear range. Based on the monitoring data of the passively controlled eight-story steel building, a data-driven stochastic subspace identification algorithm with a different strategy to remove spurious modes is used to extract dynamic properties of the passively-controlled eight-story steel building from the recorded floor acceleration data. Then, the inherent damping characteristic of the building is identified under various earthquakes. Besides, the variation of the estimated natural frequencies, mode shapes, and damping ratios for all the earthquake recordings are illustrated.

To further investigate serviceability of the passively-controlled steel building during an earthquake, probabilistic model updating is developed to estimate the model parameters and infer structural response. Bayesian inference framework has recently been used for updating a model using the identified modes [33, 39]. However, sensors were placed on selected floors due to the cost of structural health monitoring, and the identified mode shapes were only available for the measured floors with sensors, which are typically required by Bayesian model updating. To address this challenge, a model reduction approach is introduced to

the Bayesian model updating algorithm [40–43] considering the available measurements. Then, a Markov chain Monte Carlo algorithm is employed to approximate the model parameters and qualify the model uncertainty. Furthermore, seismic performance assessment of the passively-controlled steel building stemmed from the estimated dynamic characteristics and model parameters during service period is discussed.

2. Description of Building and Structural Monitoring System

2.1. Overview of the Building and Structural Monitoring System. The monitored structure is an eight-story administration building on the main campus of the Tohoku Institute of Technology (Figure 1(a)). As seen in Figure 1(b), the structure is 48 meters long, 9.6 meters broad, and 34.2 meters tall, with 10 bays in the longitudinal direction and three bays in the transverse direction. The superstructure is made up of a steel-frame structure with precast concrete slabs, and the one-story basement is made of reinforced concrete. Oil dampers link the adjacent floors through V-type steel bracing. As indicated in Figure 1(b). For the first level (Type I) and the third to eighth floors (Type II), two types of oil dampers with varying stroke limits and orifice specifications are employed. The first floor and second floor are merged to form a large space with a height of 8 m [44].

The building has been instrumented a seismic monitoring system since it was constructed in 2003. The seismic monitoring system consists of 4 triaxial accelerometers (3 accelerometers on the structure and 1 accelerometer on the ground near the building). Servo-type accelerometers were placed on the first, fourth, and eighth floors. Displacement meters and strain gauges were also mounted to measure damper brace story drifts, axial deformations, and axial forces. In 2016, the vibration sensors were rearranged with each triaxial accelerometer placed on the first, third, sixth, and eighth floor, respectively. The type of sensors and their locations are deployed in Figure 1(c). Small servo accelerometers were employed to record floor accelerations. Besides, the seismic reactions were captured and saved on a server for later study. Horizontal accelerations were measured in east-west (EW) and north-south (NS) directions, which correspond to the building's longitudinal and transverse directions, respectively. More details of the building and the instrumentation have also been described in [45].

2.2. Characteristics of Recorded Seismic Responses. The Great East Japan Earthquake struck northeastern Japan with a moment magnitude of 9.0 on March 11, 2011, the largest ever recorded in Japan. The passively-controlled steel building survived the earthquake without structural damage. However, all oil dampers on the first floor were entirely wrecked due to abutment breakage, and all dampers on the third and fourth floors experienced serious oil leaks. After postearthquake investigation, the insufficient stroke limit is

the main cause of the collision between the damper and the abutment on the floor, which finally led to the failure of the oil dampers. To accommodate larger interstory drifts, a novel retrofit plan was proposed with tin-rubber bearings replacing the damaged oil dampers [46]. The retrofit plan was divided into two phases: (1) the reassembled oil dampers of the 3rd and 4th floors with viscous oil refilled were reinstalled in September 2012. After that, the building experienced an earthquake; (2) it was not until the middle of Feb 2013 that the installation of tin-rubber bearings was completed. Thus, the recorded seismic responses corresponding to different damping provide valuable information about the state of the building as well as the damper devices. A total of 21 seismic events were recorded during 2003 and 2017, and the retrofitted building with isolators on the 1st floor and oil dampers on the 3rd~8th floors are shown in Figure 2.

The recorded earthquakes occurred in Sendai located in the Miyagi Prefecture of Japan, and detail specifications in terms of their time, date, location, depth, and epicentral distance, as well as magnitude for strong earthquake are listed in Table 1.

The recorded seismic response signals are processed through a 20th-order lowpass Butterworth filter with a cut-off frequency of 20 Hz, and the cut-off frequency of 20 Hz is far from the natural frequencies of interest, which are generally in the lower-frequency region up to 6 Hz. Then, the recorded seismic responses of the building measured by the structural health monitoring system between 2003 and 2017 are listed in Table 2. The response amplification of the both top stories and first floor in the EW and NS directions can be observed in Table 2. The peak accelerations on the eighth floor of the building in the EW and NS directions were around 2 times of the ground acceleration on average under large recorded seismic response. Figure 3 depicts magnitude and phase of the transfer functions of the building in both EW and NS directions, which give perspective to the variation of the natural frequency and damping. The peaks of transfer functions of the building vary obviously after March 11, 2011. The detailed reason for this phenomenon will be investigated and illustrated. Besides, the influence of the response amplitude on the estimated parameters is also presented.

3. Data-Driven Stochastic Subspace Identification Methodology

3.1. Data-Driven Stochastic Subspace Identification Algorithm. The stochastic subspace state-space system identification technique is developed and employed in this study. In this method, the structure can be represented as a discrete time, time-invariant structural system, which can be expressed as follows:

$$x_{k+1} = Ax_k + Bu_k + w_k, \quad (1)$$

$$y_k = Cx_k + Du_k + v_k,$$

where $y \in \mathbb{R}^{m \times 1}$ represents the output vector, $x \in \mathbb{R}^{n \times 1}$ denotes the state vector, u is the input vector, k denotes the k th time interval, and w and v represent the process noise

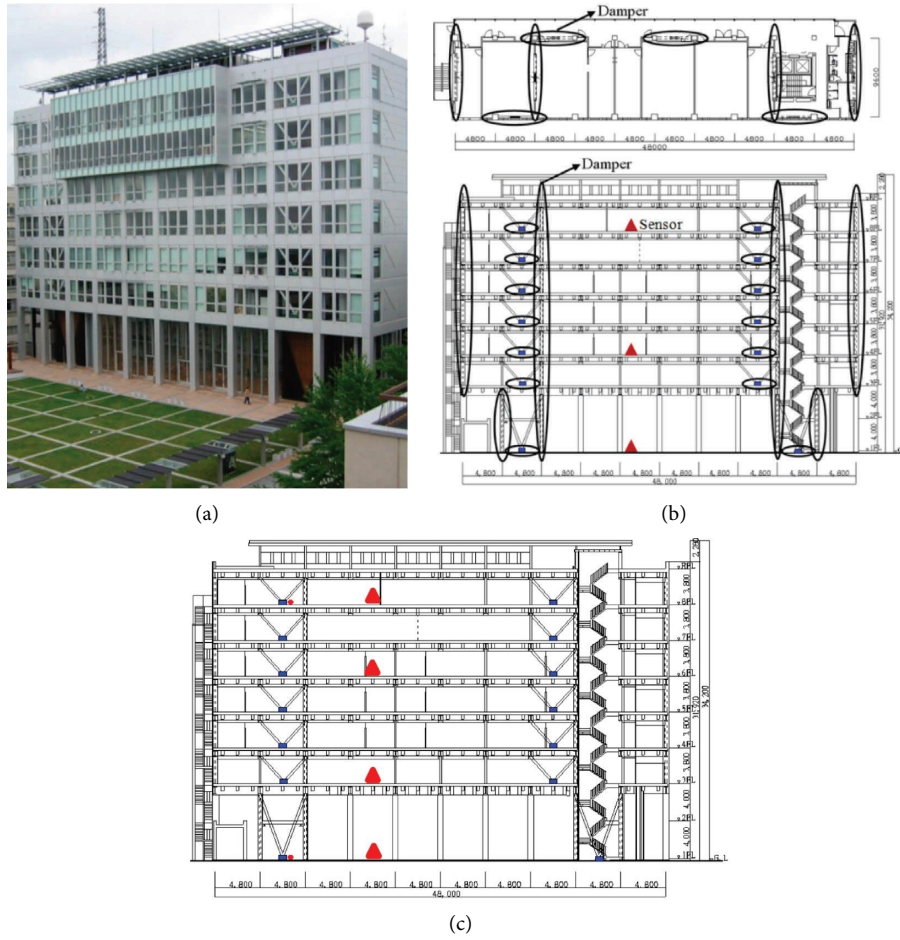


FIGURE 1: The administration building (blue square represents damper, red dot represents load cell, and red triangle represents accelerometers). (a) Front view. (b) Allocation of oil dampers and accelerometers. (c) Reallocation of oil dampers and accelerometers (after 2016).

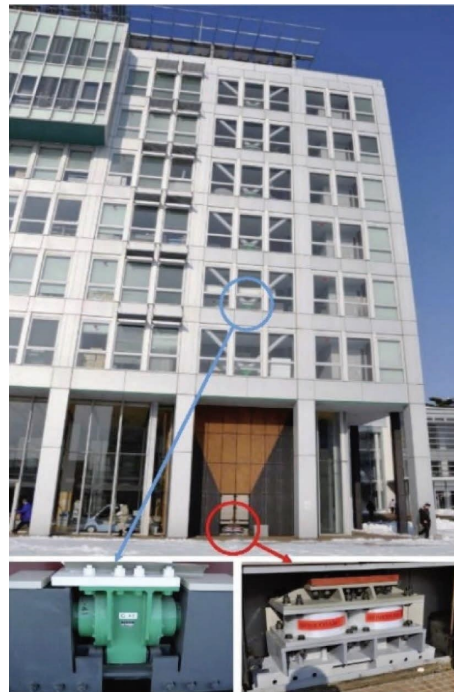


FIGURE 2: Retrofitted building with isolators on the 1st floor and oil dampers on the 3rd~8th floors.

TABLE 1: Information of earthquakes.

Date (y/m/d)	Time (UTC)	Location		Epicentral distance (km)	Depth (km)	Magnitude (M)
		N (°)	E (°)			
2003/5/26	9:24:33	38.849	141.568	88.6	68	7
2005/8/16	2:46:28	38.276	142.039	102.1	36	7.2
2010/6/13	3:32:57	37.372	141.625	119.7	27	5.9
2011/3/9	2:45:20	38.435	142.842	173	32	7.3
2011/4/7	14:32:43	38.276	141.588	62.7	42	7.1
2013/8/4	3:28:50	38.213	141.862	86.9	56	5.8

TABLE 2: Seismic response records of the building measured by the structural health monitoring system.

Recorded time	Peak response			
	EW-direction (cm/s ²)		NS-direction (cm/s ²)	
	First floor	Top floor	First floor	Top floor
Record 2003/05/26	90.77	158.53	114.16	120.79
Record 2005/08/16	88.68	158.87	103.67	125.84
Record 2010/06/13	31.77	43.03	63.86	65.62
Record 2011/03/09	27.30	126.55	30.90	85.90
Record 2011/03/24	32.15	67.44	25.74	57.74
Record 2011/04/07	160.19	308.69	175.35	258.75
Record 2012/12/07	45.21	91.14	55.96	92.87
Record 2013/08/04	29.60	33.83	35.07	42.43
Record 2014/02/06	3.63	13.63	5.39	9.83
Record 2014/02/08_0218	5.94	5.41	8.99	6.72
Record 2014/02/08_1141	3.41	4.75	3.95	3.66
Record 2014/06/09	9.60	5.51	10.28	6.69
Record 2014/06/15	3.48	4.03	4.56	7.67
Record 2014/06/16	19.12	30.61	20.46	25.61
Record 2014/11/20	7.86	9.07	6.38	11.36
Record 2015/02/17	7.94	27.71	8.76	31.07
Record 2015/05/13	5.49	5.82	6.42	6.77
Record 2016/11/12	16.91	22.25	16.07	16.60
Record 2016/11/22	36.97	66.86	41.46	66.46
Record 201612/31	10.09	17.30	9.89	22.29
Record 2017/02/28	26.12	43.00	24.37	23.80

and measurement noise, respectively. Both w and v are assumed to be zero-mean, stationary, and white-noise vector sequences. Matrices A (dynamical system matrix), B (input matrix), C (output matrix), and D (feed through matrix) are system parameters matrix of the state space model.

Basic idea of subspace methods is first to compute the estimate of state vectors from an observed input-output data and define the block Hankel matrices as follows:

$$\begin{bmatrix} U_p \\ U_f \end{bmatrix} = \begin{bmatrix} u_1 & u_2 & \cdots & u_j, \\ u_2 & u_3 & \cdots & u_{j+1}, \\ \vdots & \vdots & \ddots & \vdots, \\ u_i & u_{i+1} & \cdots & u_{i+j-1}, \\ u_{i+1} & u_{i+2} & \cdots & u_{i+j}, \\ u_{i+2} & u_{i+3} & \cdots & u_{i+j+1}, \\ \vdots & \vdots & \ddots & \vdots, \\ u_{2i} & u_{2i+1} & \cdots & u_{2i+j-1}. \end{bmatrix} = \begin{bmatrix} u_1 & u_2 & \cdots & u_j, \\ u_2 & u_3 & \cdots & u_{j+1}, \\ \vdots & \vdots & \ddots & \vdots, \\ u_{i+1} & u_{i+2} & \cdots & u_{i+j}, \\ u_{i+2} & u_{i+3} & \cdots & u_{i+j+1}, \\ u_{i+3} & u_{i+4} & \cdots & u_{i+j+2}, \\ \vdots & \vdots & \ddots & \vdots, \\ u_{2i} & u_{2i+1} & \cdots & u_{2i+j-1}. \end{bmatrix} = \begin{bmatrix} U_p^+ \\ U_f^- \end{bmatrix} \in \mathbb{R}^{2m \times j}, \quad (2)$$

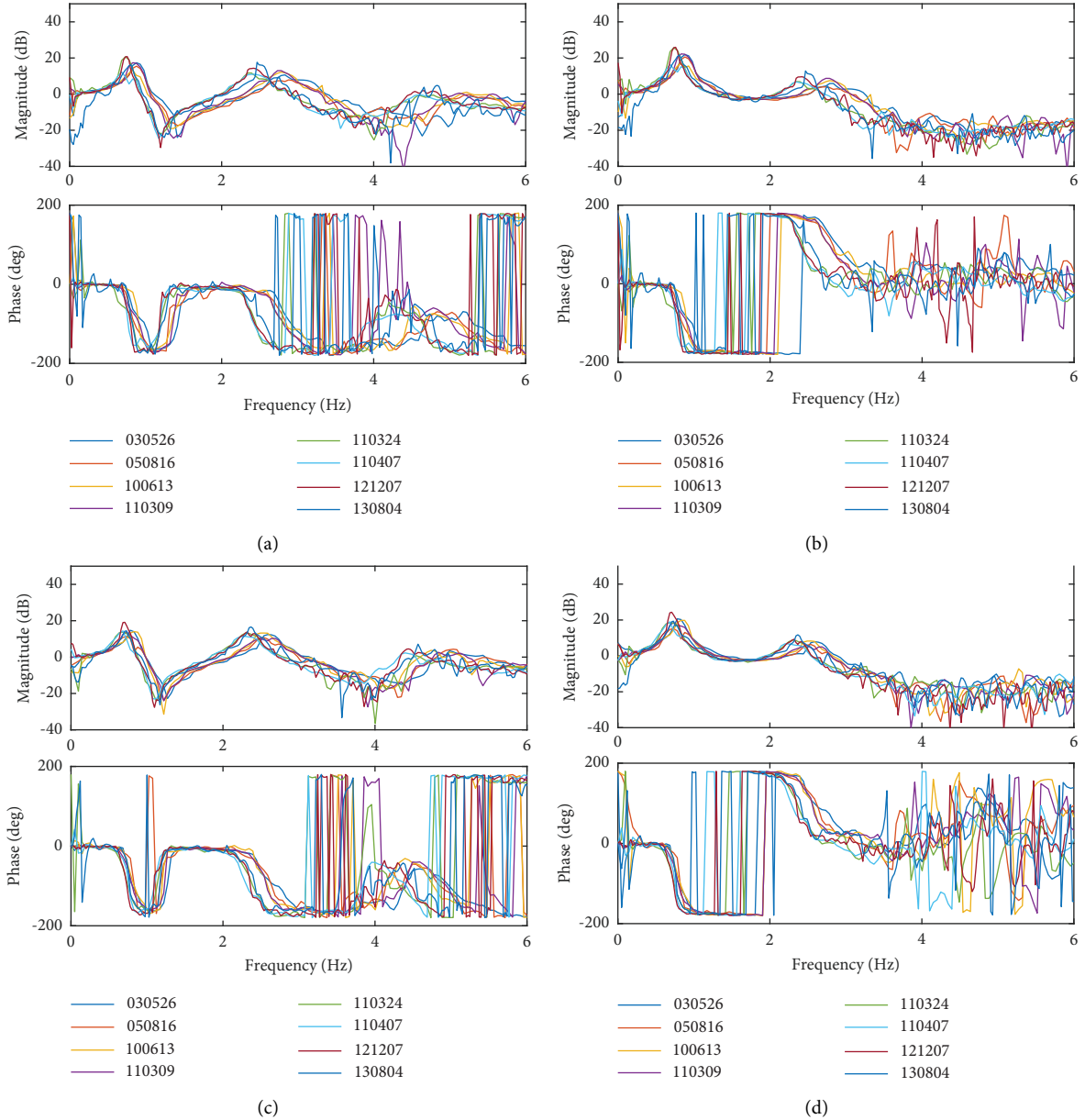


FIGURE 3: Transfer functions of accelerations of the building in the EW and NS directions. (a) Transfer function between 1st floor and 4th floor (EW). (b) Transfer function between 1st floor and 8th floor (EW). (c) Transfer function between 1st floor and 4th floor (NS). (d) Transfer function between 1st floor and 8th floor (NS).

where $U_p \in \mathbb{R}^{m \times j}$ and $U_f \in \mathbb{R}^{m \times j}$ denote the past and future input Hankel matrix, respectively. $U_p^+ \in \mathbb{R}^{m(i+1) \times j}$ and $U_f^- \in \mathbb{R}^{m(i-1) \times j}$ are hence used to represent the past and future input Hankel matrix with adding and reducing one block row, respectively. Similarly, the output Hankel matrix (Y_p and Y_f) can be instituted the same way. Then, the LQ decomposition was implemented to a special Hankel matrix as follows:

$$\begin{bmatrix} U_f \\ W_p \\ Y_f \end{bmatrix} = \begin{bmatrix} R_{11} & 0 & 0 \\ R_{21} & R_{22} & 0 \\ R_{31} & R_{32} & R_{33} \end{bmatrix} \begin{bmatrix} Q_1^T \\ Q_2^T \\ Q_3^T \end{bmatrix}, \quad (3)$$

where $W_p = \begin{bmatrix} U_p \\ Y_p \end{bmatrix} \in \mathbb{R}^{(m+1) \times j}$, oblique projection method is generally used to solve equation (3), and hence the oblique projection P of the future Y_f onto the joint past W_p along the U_f could be obtained from the LQ decomposition as follows:

$$P = R_{32} R_{22}^\dagger W_p, \quad (4)$$

where R_{22}^\dagger denotes the pseudoinverse of matrix R_{22} . The main theorem of subspace identification states that the projection matrix P can be factorized into the product of the extended observability matrix \mathcal{O} and future state vector X_f

(Van Overschee and De Moor 1996); that is, the projection matrix P can also be expressed as follows:

$$P = R_{32}R_{22}^\dagger W_p = \mathcal{O}X_f. \quad (5)$$

Assuming that the singular value decomposition (SVD) of P is given as $P = U\Sigma V^T$, the rank of the projection matrix P equals to the rank of matrix Σ , i.e., $\text{rank}(P) = \text{rank}(\Sigma)$, and let the extended observability matrix \mathcal{O} be as follows:

$$\mathcal{O} = U\Sigma^{1/2}. \quad (6)$$

Once the extended observability matrix \mathcal{O} is obtained, the system matrices A and C can be determined as follows:

$$A = \mathcal{O}(1:n(L-1), :)^{\dagger} \mathcal{O}(n+1:nL, :), C = \mathcal{O}(1:m, 1:n). \quad (7)$$

Then, natural frequency, damping ratio, and mode shape of the i th mode of the system can be estimated by solving the eigenvalues problem of matrix A as follows:

$$A\Psi = \Lambda\Psi, \quad (8)$$

$$\Lambda = \text{diag}(\tilde{\lambda}_i), \quad (9)$$

where matrices Λ and Ψ are the eigenvalues and eigenvectors of matrix A , respectively. $\tilde{\lambda}_i$ denotes diagonal eigenvalues element of matrix Λ . After implementing z-transform to eigenvalues $\tilde{\lambda}_i$, natural frequency, damping ratio, and the mode shape of the i th mode of the system can be estimated as follows:

$$\lambda_i = \frac{\ln(\tilde{\lambda}_i)}{\Delta t}, \quad (10)$$

$$\omega_i = \sqrt{\text{Real}(\lambda_i)^2 + \text{Image}(\lambda_i)^2}, \xi_i = \frac{\text{Real}(\lambda_i)}{\omega_i}, \quad (11)$$

$$\Phi = C\Psi. \quad (12)$$

Generally, there is a common difficulty in selecting appropriately size of the system order, which is nontrivial and crucial for successfully identifying the inherent damping characteristic of the building in this subspace identification algorithm. As a result, a common practice is that the system order will be overestimated in order to avoid losing any physical modes and mode bias error [47]. Since this practice may introduce numerical modes, stabilization diagram that reflects the variation of the estimated modal parameters with model order increments is usually employed to distinguish real modes from spurious ones generated during system identification. However, there are still some challenges that the stabilization diagram method cannot cope with. One is to select an unbiased preassigned system order; the other is the variance of identified real system modes under different system orders.

In this paper, a different approach of constructing the system matrix A is adopted as validation criteria to overcome the drawbacks of traditional stabilization diagram method [13]

$$A = \{\mathcal{O}(1:n(L-1), :)^T \mathcal{O}(n+1:nL, :)\}^{-1} \{\mathcal{O}(1:n(L-1), :)^T \mathcal{O}(1:n(L-1), :)\}, \quad (13)$$

where L represents the order of Toeplitz matrix and n denotes the number of measurements. Two groups of natural frequency f_{i1} and f_{i2} , damping ratio ξ_{i1} and ξ_{i2} , and mode shape Ψ_{i1} and Ψ_{i2} of the i th mode of the system under the same assumed system order are calculated by using equations (6)–(13), respectively. A real mode can be estimated, if it is able to be identified consistently by the above two approaches. Therefore, real modes can distinguish themselves from the spurious modes through the modal property comparison of these two groups. For practical application, thresholds are also assigned to check the consistency of the modal properties derived from the above two approaches, which can be calculated as follows:

$$\begin{aligned} \left| \frac{f_{i1} - f_{i2}}{f_{i1}} \right| &< f_{\text{threshold}}, \\ \left| \frac{\xi_{i1} - \xi_{i2}}{\xi_{i1}} \right| &< \xi_{\text{threshold}}, \end{aligned} \quad (14)$$

$$\left| \frac{\Psi_{i1}^T \Psi_{i2}}{\|\Psi_{i1}\|^{0.5} \|\Psi_{i2}\|^{0.5}} \right| > \text{MAC}_{\text{threshold}},$$

where ψ is the mode shape and subscript 1 and 2 denote a certain mode evaluated from equations (6)–(9), respectively.

To consistently pick the “genuine” modes, the stabilization diagram is used to distinguish true modes from false ones. The stabilization diagram can depict the relative differences between each mode. As a result, by comparing the dynamic features of these two approaches, true modes can be distinguished from spurious modes. Nevertheless, mathematical mode may pass the stabilization criteria in few special cases. A different approach of constructing the system matrix A is proposed as validation criteria to remove the above mathematical mode. The relative differences, which are used to assess the consistency of the modal properties produced from two methodologies, are often defined as less than 1% for the natural frequencies, less than 5% for damping ratios, and 10% for the modal assurance criterion (MAC) index of mode shapes. In addition, modal phase collinearity (MPC) index is also employed as validation criteria [24] in this study.

3.2. Implementation and Identification Results. The subspace identification technique was implemented to acceleration response records of the building spanning from 2003 to

2017, and a total of 21 events were selected for analysis. As all the recordings are in discrete time domain, the discrete time subspace identification method was adopted. To implement the data-driven stochastic subspace identification methodology with a different strategy to remove spurious modes of the system, the seismic acceleration response records on the 1st floor were selected as the input, while the accelerations from the upper stories were utilized as outputs. Noteworthy, there is no need to consider the effect of soil-structure interaction, since 1st floor acceleration response was considered as the input excitation rather than the free-field ground acceleration records.

The identified stable modes are presented in Figures 4 and 5 for EW and NS direction, respectively, which also depicts the estimated transfer function curve as comparison.

3.3. Analysis of the Passively-Controlled Steel Building.

The seismic acceleration responses of the passively-controlled steel building recorded from 2003 to 2017 (a total 21 events) are used for analysis. From the identification results shown in Figures 4 and 5, the first two stable modes can be observed for almost every earthquake event, while the third stable mode can only be estimated for several earthquake events. This is a common phenomenon for structures in civil engineering that the low-order modal responses are very often excited by an earthquake, and the high-order modal responses are not that easily excited by an earthquake. Furthermore, identifiability of high-order modes gets even worse, as their modal responses and signal-to-noise ratios decrease gradually as the modal order increases [48, 49]. Then, the distribution of the identified fundamental frequencies and damping ratios corresponding to every seismic event for both longitudinal and transverse direction are depicted in Figure 6. As can be observed that estimated uncertainty of damping ratios is distinctly large than that of natural frequency due to the complexity of actual structural damping, and the modal damping is only a mathematical concise expression, which may not be able to completely and accurately simulate the complex damping mechanism of the actual structure. In addition, the corresponding peak ground acceleration (PGA) of each seismic event is also shown in Figure 6. As can be seen, most of the earthquake excitation levels (input PGA) for these recorded seismic events are less than 50 gal except three strong seismic events in this study.

The variation of the identified fundamental modes of the building is quite obvious based on the results of the identification. Detailed investigation is necessary due to energy dissipation devices of the passively-controlled steel building. Considering the changes of the energy dissipation device before and after the Great East Japan Earthquake is significant, the identified natural frequencies of the building can hence be divided into two parts: One is before the Great East Japan Earthquake, and the other is after the restoration. The natural frequencies show a slight decrease; then, both natural frequencies and damping ratios are basically stable during the period between 2003 and 2010, when earthquake excitation level that struck the building is relatively small. On the contrary, the natural frequencies and damping ratios

identified from seismic event on March 24, 2011, show a sharp decline. These declines are coincident with the phenomena that most of oil dampers have damaged or severe oil leakage after March 11, 2011. Progressive increases of natural frequencies and damping ratios were observed during the two-stage retrofit.

To further study the phenomena, first two fundamental frequencies and damping ratios identified for each seismic event are illustrated in Figure 7 for longitudinal and transverse directions, respectively. Figures 7(a) and 7(b) display that the natural frequencies and first damping ratio identified from seismic events before March 11, 2011, remained nearly constant under moderate levels of vibration amplitudes; meanwhile, the second damping ratio shows a slight decrease with declined vibration amplitudes. After March 11, 2011, the natural frequencies decreased by 12.6% and 11.7% on the average of the first two modes in longitudinal and transverse directions, respectively, which indicates the fact that oil damper braces could also offer additional dynamic stiffness. Moreover, due to half of the oil dampers lost damping capability, the damping ratios decreased by 35.6% and 40.4% on the average of the first two modes in longitudinal and transverse directions. Additional damping ratio provided by original oil dampers was thus taken to be around 2%. Subsequently, the building was retrofitted with tin-rubber bearings replacing the oil dampers in the first floor; after completely repairing, natural frequencies and damping ratios recovered to a certain level but not as initial.

Figures 7(c) and 7(d) reveal the dynamic properties of the building with hybrid energy dissipating device. The identified first two natural frequencies remained nearly constant under almost the similar level of earthquake excitation and slightly decreased with increasing vibration amplitudes, whereas the damping ratios increased significantly along with the increasing vibration amplitudes. This was attributed to the inelastic response of the tin-rubber bearings.

Detailed analysis is also conducted considering the combination of tin-rubber bearings with oil dampers in this building. The correlation among identified system natural frequencies, damping ratios, and PGA is depicted in Figures 8(a) and 8(b). As can be observed, the first two natural frequencies belonging to longitudinal and transverse directions slightly decrease with increasing earthquake excitation level (input PGA). On the contrary, damping ratio increases with rising PGA. Figures 8(c) and 8(d) also display the plot of damping ratios for longitudinal and transverse directions and the plot of damping ratio versus natural frequency. The relationship between the recorded PGA and response peak acceleration (PA), namely, acceleration magnification ratio, for each event in longitudinal, transverse, and vertical directions is shown in Figure 9. Figure 9 shows that the PGA value is inversely proportional to the PA value. It can also be observed that acceleration magnification ratio (AMR) of the building after retrofitting with tin-rubber bearings is less than ever before. The decreased AMR reflects better seismic resistance performance after retrofit. The AMR in vertical direction is distinctly greater than that

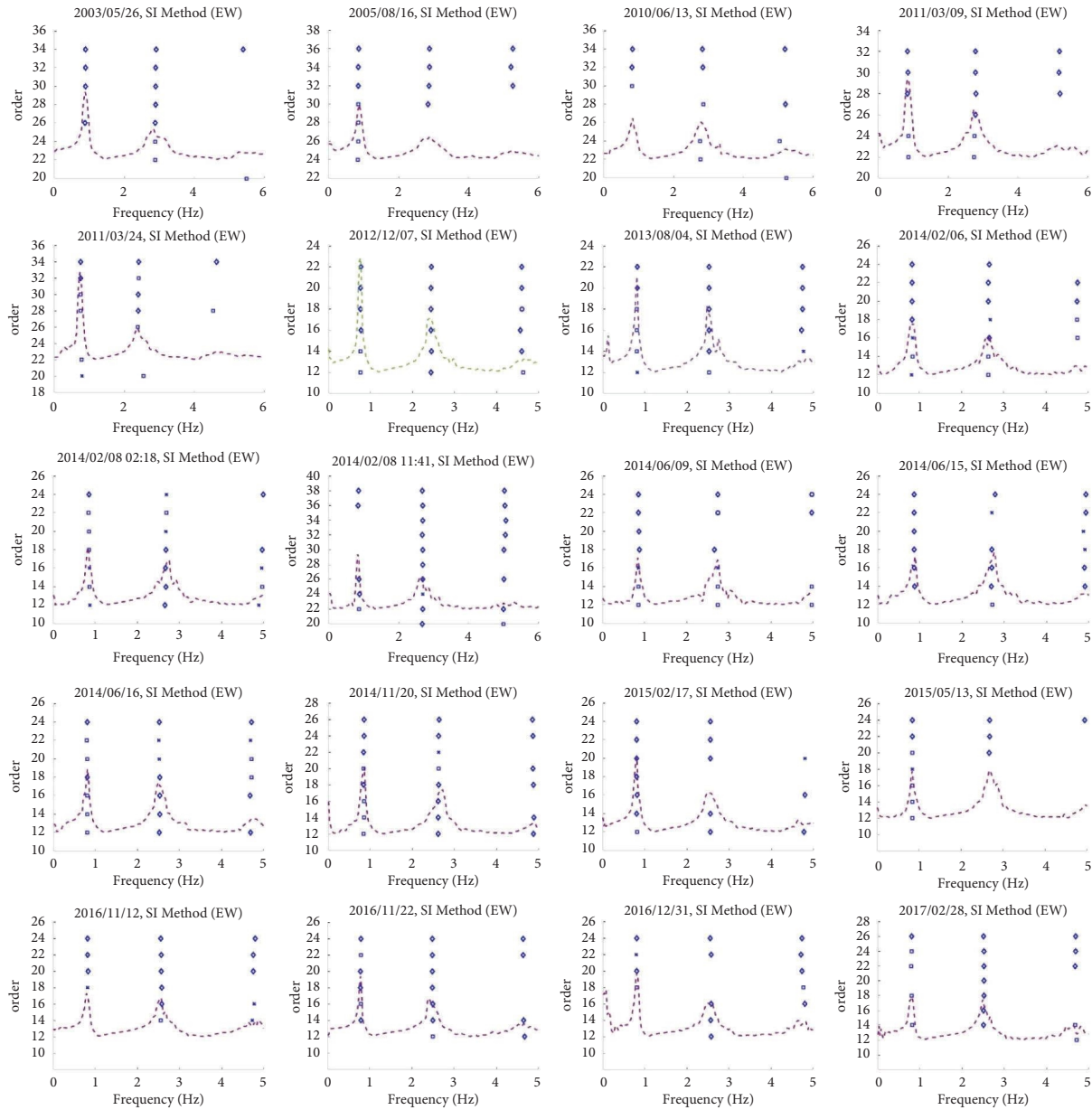


FIGURE 4: Stable diagrams for all earthquake records in EW (dotted lines represent the corresponding transfer function).

in horizontal direction (as shown in Figure 9(b)). This indicates that the isolation bearings can effectively reduce the acceleration response of the building for horizontal direction rather than vertical direction.

4. Probabilistic Model Updating

Structural model updating is crucial for structural health monitoring and control, as it is generally concerned with evaluating structural health condition, dynamic responses, and remaining lifetime [25–27]. As there are emerging needs for the calibrating structural model, Bayesian inference framework has recently been proposed to update structural

model and accommodate modeling uncertainties of the structural system using the identified modes [33, 39]. However, sensors were placed on selected floors due to the cost of structural health monitoring, and the identified mode shapes were only available for the measured floors with sensors, which are typically required by Bayesian model updating. To address this challenge, a model reduction approach is introduced to the Bayesian model updating algorithm [40–43] considering the available measurements. Then, a Markov chain Monte Carlo algorithm [38] is employed to approximate the model parameters and qualify the model uncertainty. Furthermore, seismic performance assessment and structural response prediction of the

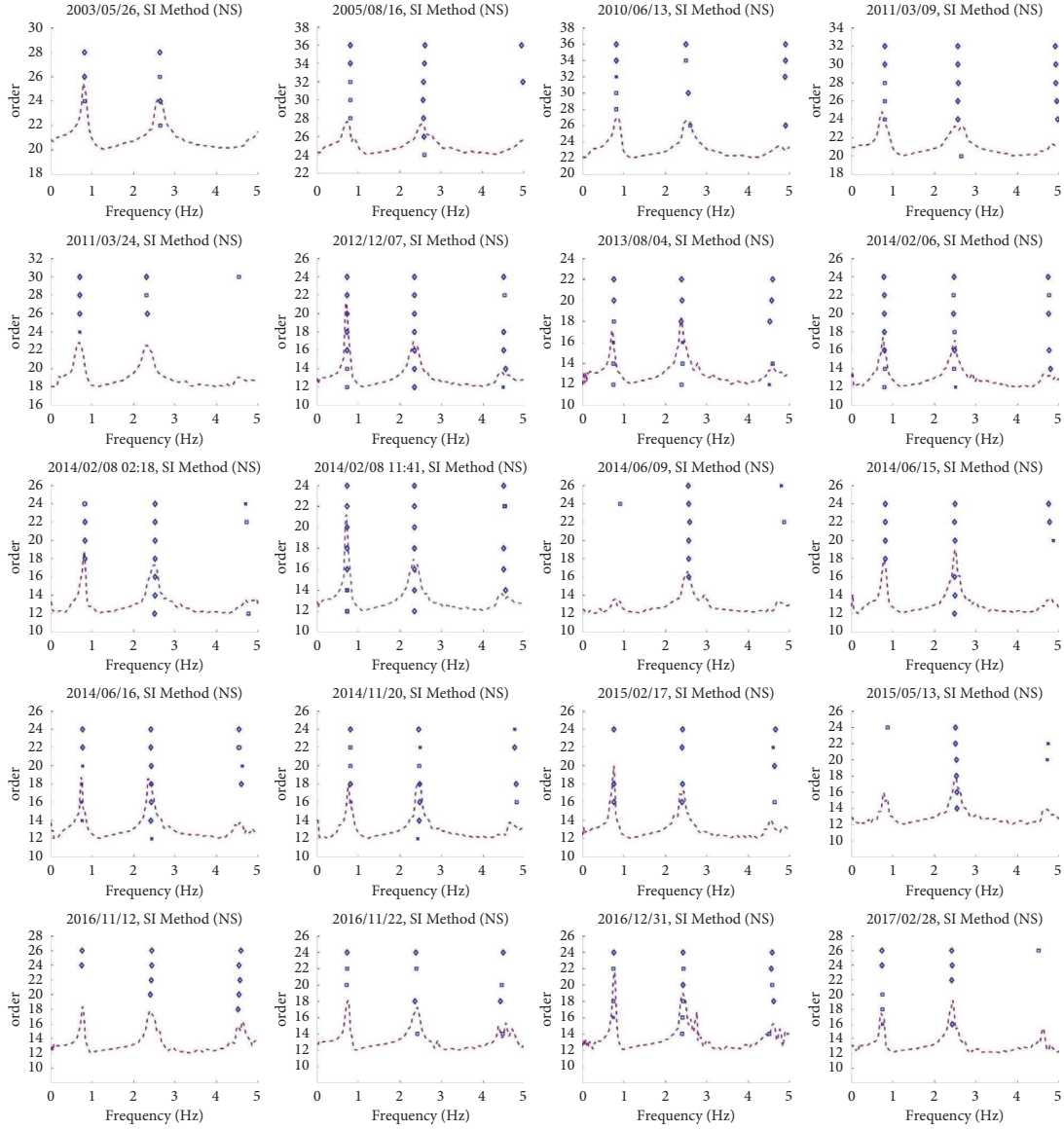


FIGURE 5: Stable diagrams for all earthquake records in NS (dotted lines represent the corresponding transfer function).

passively-controlled steel building stemmed from the estimated dynamic characteristics and model parameters during service period are conducted.

4.1. Bayesian Inference for Model Updating. In this study, the structural dynamic model for the generalized passively-controlled structure can be represented as follows:

$$M(\theta)\ddot{x}(t) + C(\theta)\dot{x}(t) + K(\theta)x(t) + f_d(\theta, x(t), \dot{x}(t)) = -M\ddot{x}_g(t), \quad (15)$$

where $M(\theta) \in \mathbb{R}^{n \times n}$ denotes the mass matrix, $C(\theta) \in \mathbb{R}^{n \times n}$ represents the damping matrix, and $K(\theta) \in \mathbb{R}^{n \times n}$ is the stiffness matrix, which are all parameterized by a set of model parameters $\theta \in \mathbb{R}^{n_\theta \times 1}$ (where n_θ denotes the number of parameters). n denotes the degrees-of-freedom (DOFs).

Following the Bayes' theorem, posterior probability density function (PDF) of θ yields the following equation:

$$p(\theta | \mathcal{D}) = c^{-1} p(\mathcal{D} | \theta) p(\theta), \quad (16)$$

where c is a normalizing factor and represents the evidence providing the data set \mathcal{D} , which can be expressed as follows:

$$c = \int p(\mathcal{D} | \theta) p(\theta) d\theta, \quad (17)$$

where $p(\theta)$ is the prior probability density function and represents the initial guess about the distribution of θ , $p(\theta | \mathcal{D})$ is the posterior PDF of θ given on measured data set \mathcal{D} , and $p(\mathcal{D} | \theta)$ denotes the likelihood function.

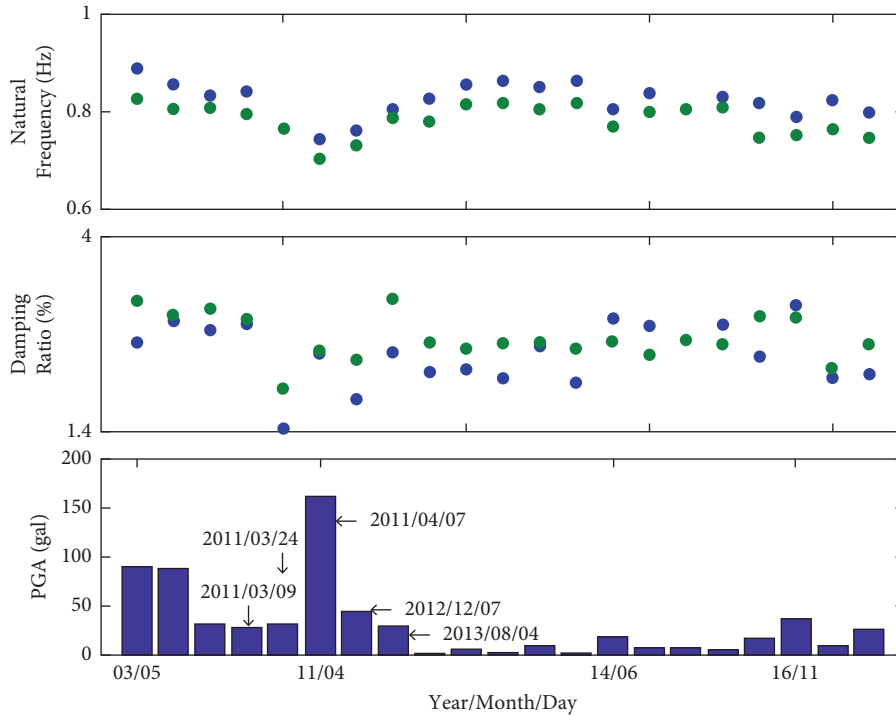


FIGURE 6: Plot of the identified system natural frequencies and damping ratios of the building with respect to each seismic event (green dot represents transverse direction and blue dot denotes longitudinal direction).

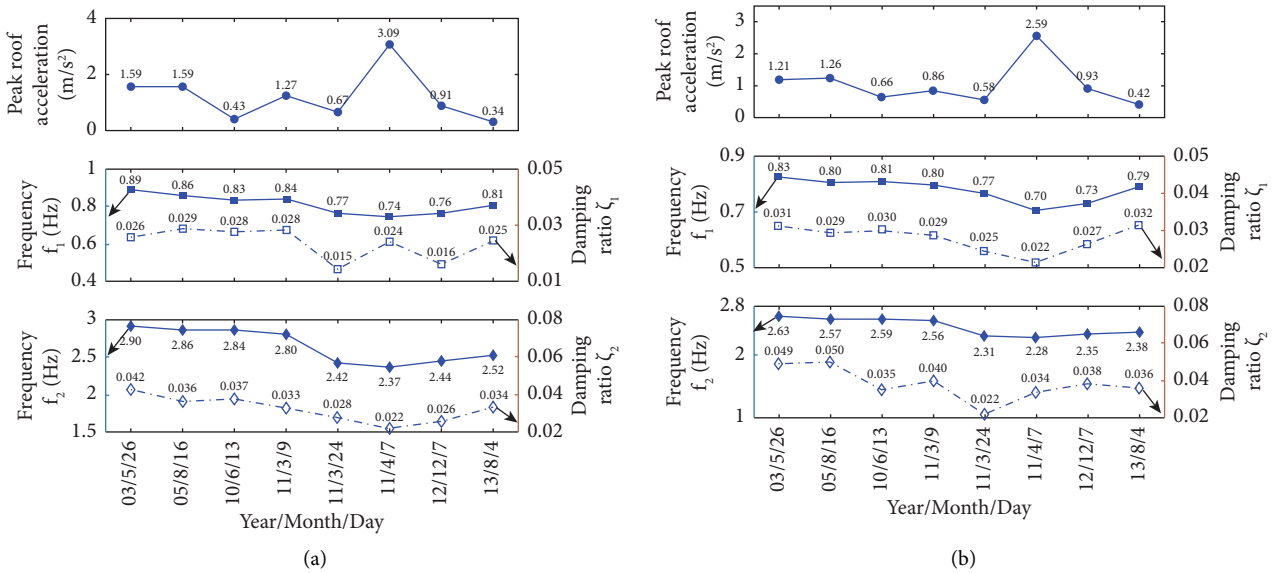
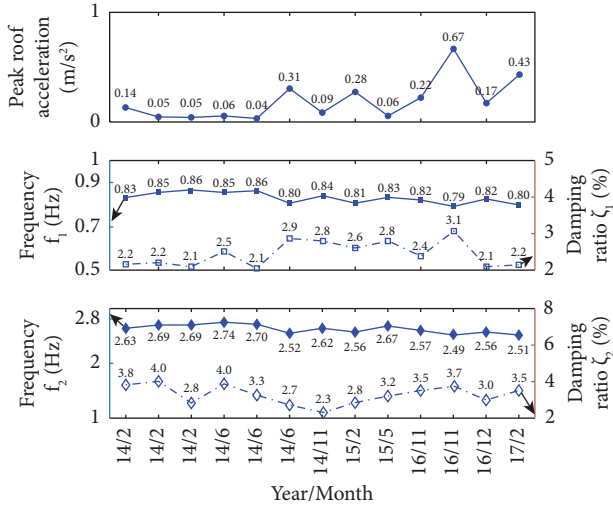
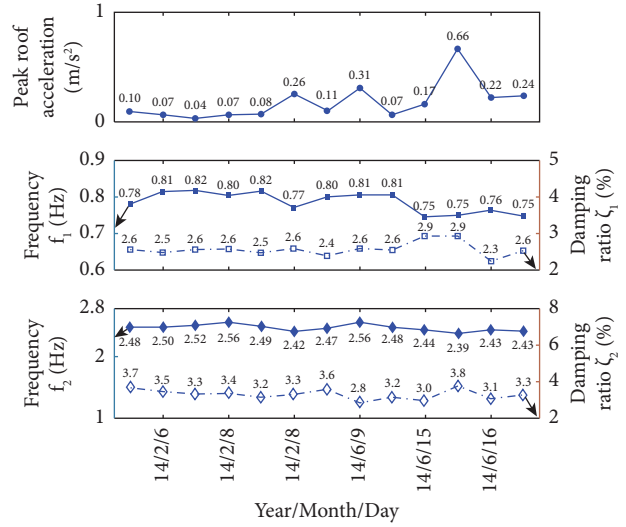


FIGURE 7: Continued.

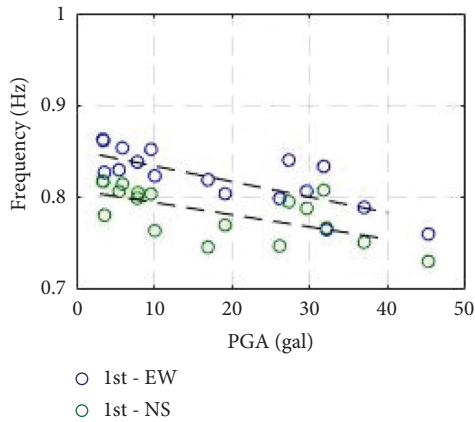


(c)

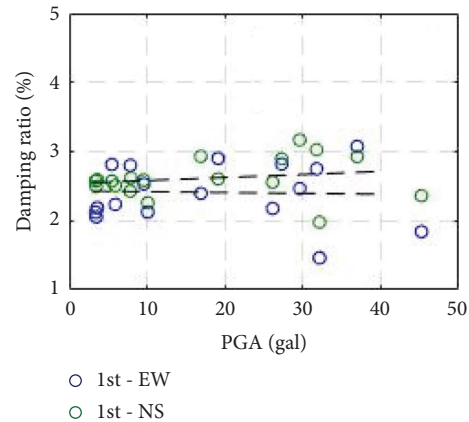


(d)

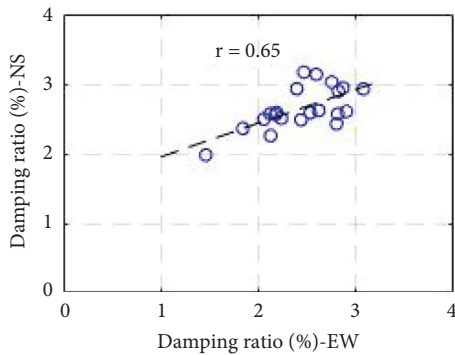
FIGURE 7: Identified system natural frequencies and damping ratios of the building. (a) From 2003 to 2013 in EW direction. (b) From 2003 to 2013 in NS direction. (c) From 2014 to 2017 in EW direction. (d) From 2014 to 2017 in NS direction.



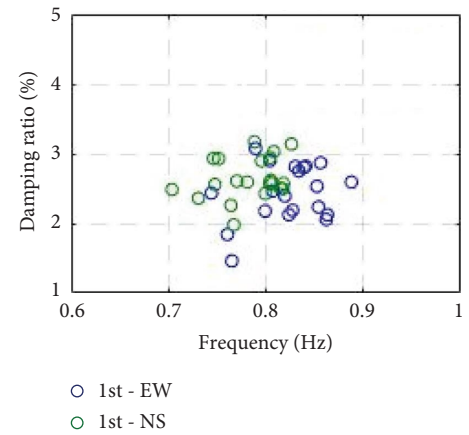
(a)



(b)



(c)



(d)

FIGURE 8: (a) Relationship between PGA and identified natural frequency for longitudinal and transverse directions. (b) Relationship between PGA and damping ratio for longitudinal and transverse directions. (c) Correlation between damping ratios for longitudinal and transverse directions. (d) Relationship between damping ratio and natural frequency for longitudinal and transverse directions.

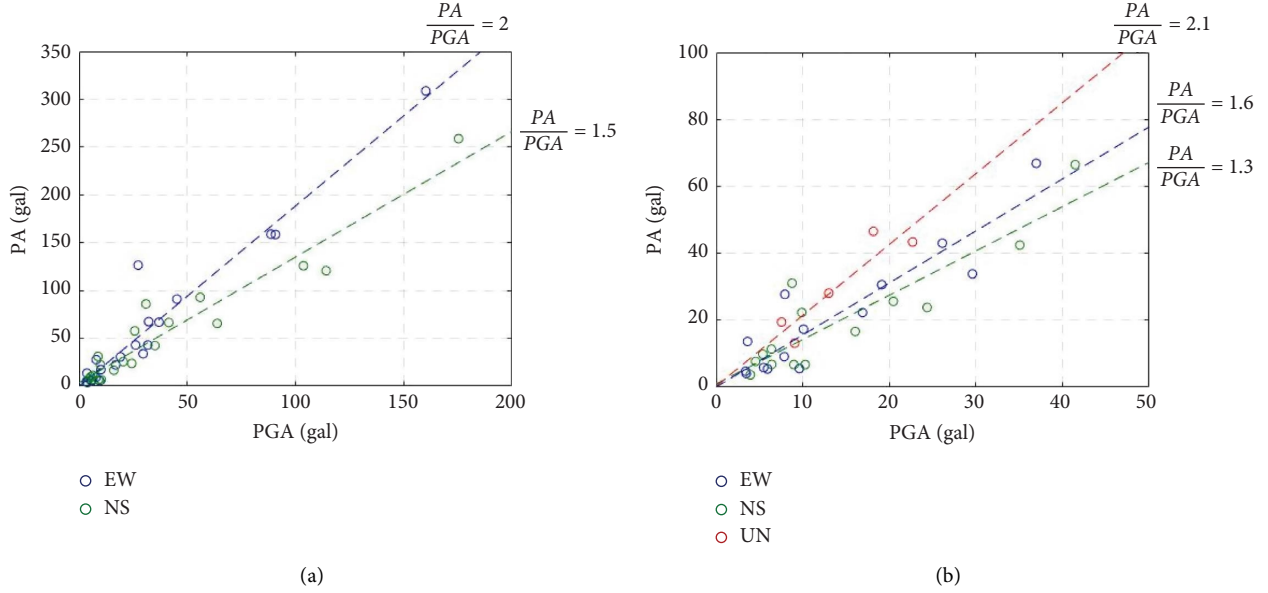


FIGURE 9: Relationship between PGA and maximum peak acceleration (PA) (EW denotes longitudinal direction, NS is transverse direction, and UN represents vertical direction).

Furthermore, the likelihood function can be established through defining the model prediction error ε to measure the agreement between measured and predicted data, which can be written as follows:

$$\varepsilon = y - \hat{y}. \quad (18)$$

From Jaynes' principle of maximum (information) entropy, Gaussian probability model is employed to characterize model prediction error ε , as Gaussian distribution can give the maximum uncertainty for parameters θ . Thus, prediction error ε follows a zero-mean Gaussian distribution, i.e., $\varepsilon \sim N(0, \Sigma_e) = N(0, \sigma_j^2 I)$, where Σ_e denotes the unknown covariance matrix, σ_j^2 is the j th variance of the prediction error, and $I \in \mathbb{R}^{N_m \times N_m}$ represents an identity matrix (N_m is the number of the observed DOFs). Thus, the likelihood function can be written as follows:

$$p(\mathcal{D} | \theta) = \frac{|\Sigma_e|^{-N/2}}{(2\pi)^{N_m N/2}} \exp\left(-\frac{[y - \hat{y}]^T [y - \hat{y}]}{2\Sigma_e}\right), \quad (19)$$

where N denotes the number of data in a data set. As can be seen that σ_j^2 is also unknown, which needs to be identified. Hence, the likelihood function needs to be revised as $p(\mathcal{D} | \theta, \sigma^2) = p(\mathcal{D} | \theta)$, where $\sigma^2 = \{\sigma_1^2, \dots, \sigma_{N_m}^2\}$. Consequently, the revised posterior PDF of augmented parameters can be estimated as follows:

$$p(\theta, \sigma^2 | \mathcal{D}) \propto p(\mathcal{D} | \theta, \sigma^2) p(\theta) p(\sigma^2), \quad (20)$$

where $p(\theta, \sigma^2 | \mathcal{D})$ is the posterior PDF of augmented parameters and $p(\sigma^2)$ represents the prior PDF of σ^2 .

Generally, the posterior PDF of parameters does not have an analytical solution except the special case, and hence stochastic simulation methods are utilized to approximate the posterior PDF of parameters. However, it is still

a challenge to sample directly from the posterior PDF of parameters as shown in equation (16). Markov chain Monte Carlo (MCMC) algorithm is able to effectively take independent samples which asymptotically follow the distribution of the target PDF when the number of Markov steps increases. Therefore, MCMC algorithm is implemented to quantify the posterior PDF of the system parameters in this paper.

The main idea for MCMC is based on constructing a Markov chain to match the distribution of the target PDF (the posterior PDF of parameters in this case). A simple implementation procedure for a typical MCMC sampling is then described as follows. Take an assumption that random samples are produced by the target distribution $\pi(\theta)$ which represents the posterior PDF $p(\theta, \sigma^2 | \mathcal{D})$, and Metropolis-Hastings algorithm produces a sequence of samples $\theta^{(p)}$ through a rejection sampling procedure. At a generic p th iterative step, a candidate θ^* is sampled from a chosen proposal $q(\theta^* | \theta^{(p-1)})$. Then, a rejection sampling procedure is conducted with an acceptance probability expressed as follows:

$$\gamma = \min \left\{ \frac{\pi(\theta^*) q(\theta^{(p-1)} | \theta^*)}{\pi(\theta^{(p-1)}) q(\theta^* | \theta^{(p-1)})}, 1 \right\}. \quad (21)$$

If the above Bernoulli trial is successful, set $\theta^p = \theta^*$; otherwise, set $\theta^p = \theta^{(p-1)}$. Noteworthy, the above rejection sampling is iterated recursively until the stationary distribution is obtained. As the initial samples are sampled from the prior distribution rather than the target posterior, there exist some nonstationary Markov steps before the special designed Markov chain exploring high probability region of target distribution. The corresponding process is referred as "burn-in," which should be discarded. Therefore,

Metropolis–Hastings acceptance ratio needs to be evaluated so that the convergence of Markov chain can be guaranteed. To obtain a well-established Markov chain, the acceptance ratio should be within the range [0.15, 0.4]. In practice, it is usual to discard the samples generated during burn-in period. Other approaches that make the acceptance ratio be close to 40% can be found in [38].

4.2. Model Reduction. In practice, most often is the case that sensors are only available on selected floors due to the cost, and hence structural responses are only available for the

measured floors with sensors. Furthermore, the identified mode shapes are also available only for the measured floors with sensors, which are typically required by Bayesian model updating [50–52]. To address this challenge, a model reduction approach [53] is introduced as follows which can reduce the full rank analytical model to a more efficient model or the measured model. Take the generalized eigenvalue equation which is partitioned into the measured and unmeasured parts as follows:

$$\begin{bmatrix} \mathbf{K}_{mm} & \mathbf{K}_{ms} \\ \mathbf{K}_{sm} & \mathbf{K}_{ss} \end{bmatrix} \begin{Bmatrix} \Phi_{mm} \\ \Phi_{sm} \end{Bmatrix} - \begin{bmatrix} M_{mm} & M_{ms} \\ M_{sm} & M_{ss} \end{bmatrix} \begin{Bmatrix} \Phi_{mm} \\ \Phi_{sm} \end{Bmatrix} \Lambda_{mm} \approx \begin{Bmatrix} 0 \\ 0 \end{Bmatrix}, \quad (22)$$

where $\Phi \in \mathbb{R}^{n \times n}$ represents the mass-normalized mode shape matrix and $\Lambda \in \mathbb{R}^{n \times n}$ denotes the diagonal eigenvalue matrix of the eigenvalues. The subscripts m and s denote the master and slave degrees of freedom (DOFs), respectively, which correspond to the measured and unmeasured DOFs. Besides, $m + s = n$, where n denotes the degrees-of-freedom (DOFs). Take $\Phi_{sm} = t\Phi_{mm}$; herein, $t \in \mathbb{R}^{s \times m}$ denotes a transformation matrix and is substituted to equation (22) as follows:

$$t = -\mathbf{K}_{ss}^{-1} \mathbf{K}_{ms}^T + \mathbf{K}_{ss}^{-1} [\mathbf{M}_{ms}^T + \mathbf{M}_{ss} t] \Phi_{mm} \Lambda_{mm} \Phi_{mm}^{-1}. \quad (23)$$

Since $\Phi = [\Phi_{mm} \Phi_{sm}]^T = [I t]^T \Phi_{mm}$, take $\Phi = T \Phi_{mm}$ and substitute it into equation (22), then multiplying equation (22) by the left yields the following:

$$\mathbf{M}_R^{-1} \mathbf{K}_R = \Phi_{mm} \Lambda_{mm} \Phi_{mm}^{-1}, \quad (24)$$

where $I \in \mathbb{R}^{m \times m}$ represents an identity matrix and M_R and K_R represent the corresponding mass and stiffness matrices of the model with order reduction and can be written as $M_R = T^T M T$ and $K_R = T^T K T$.

Thus, substituting equation (24) into equation (23), we get

$$t = -\mathbf{K}_{ss}^{-1} \mathbf{K}_{ms}^T + \mathbf{K}_{ss}^{-1} [\mathbf{M}_{ms}^T + \mathbf{M}_{ss} t] \mathbf{M}_R^{-1} \mathbf{K}_R. \quad (25)$$

As can be seen that equation (25) is an implicit function of matrix t , the solution of which can be obtained by an IIRS technique through iteration [54]. As a consequence, the solutions for reduced mass and stiffness matrices can also be given in terms of the model parameters, i.e., $K_R(\theta)$.

4.3. Implementation and Results. The measured seismic acceleration responses of the passively-controlled steel building are used for Bayesian model updating as follows: the measured seismic acceleration response of the first floor is used as input excitation and the measured seismic acceleration responses of other floors as the outputs. Since the measured seismic acceleration response of the first floor is considered as the input excitation rather than the free-field ground acceleration records, the effect of soil-structure

interaction could be ignored. Besides, the effect of torsional motion is very small due to the symmetrical plan of the building. The recorded signals were processed through a 20th-order lowpass Butterworth filter with a cut-off frequency of 20 Hz, and the cut-off frequency of 20 Hz was far from the natural frequencies of interest, which are generally in the lower-frequency region up to 6 Hz. The sampling frequency of the recorded seismic responses was 200 Hz and 100 Hz for earthquake events before 2011 and after 2012.

The initial finite element model of the building is built by Sap2000, detailed modeling process, and numerical model can be found in [63, 64]. Since the translational mode and torsional mode of the initial finite element model of the structure are independent of each other, the initial model can then be simplified to the plane frame finite element model in the longitude (EW) and transverse (NS) directions of the building. The simplified FE model contains only 7 degrees of freedom, i.e., a simple beam model. Berman direct method is used to correct the simplified initial finite element model, more details can be found in [73]. The damper is simulated by a complex model, which is a combination of a Kelvin–Voigt model and a Maxwell model in parallel [55].

The identified modal data by Section 3 for strong earthquake listed in Table 1 are utilized for structural model updating. The unknown parameters used for model updating include modal frequencies, damping ratios, and modal shape vectors as well as the variance of the prediction error. Take an assumption that the prior system parameters θ characterizing the model are independently identical distribution with each other and follow Gaussian distribution. Furthermore, since the variance of the prediction error σ^2 is positive all the time, inverse gamma distribution is hence exploited to model the prior distribution of σ^2 , that is, $p(\sigma^2) \sim \text{IG}(\alpha, \beta)$. Also, assume that the variance of the prediction error is independently identical distribution with each other, and hence the prior PDF of σ^2 can be expressed as follows:

$$p(\sigma^2) = \prod_{j=1}^{N_m} p(\sigma_j^2) = \prod_{j=1}^{N_m} \frac{\beta^\alpha}{\Gamma(\alpha)} \sigma_j^{-2(\alpha+1)} e^{-\beta/\sigma_j^2}, \quad (26)$$

where $\Gamma(\cdot)$ represents the gamma function and hyper-parameters α, β denote scale parameter and shape parameter, respectively.

$$p(\mathcal{D} | \theta) = \prod_{i=1}^{N_m} \frac{1}{(2\pi\sigma_i^2)^{N/2}} \exp\left(-\sum_{i=1}^{N_m} \sum_{j=1}^N \frac{1}{2\sigma_i^2} (\ddot{x}_i(t_j) - \hat{\ddot{x}}_i(t_j))^2\right), \quad (27)$$

where $\ddot{x}_i(t_j)$ is the measured acceleration vector and $\hat{\ddot{x}}_i(t_j)$ denotes the corresponding predicted acceleration vector, N denotes the number of data in a data set, and N_m is the number of the measured observation vectors.

In the updating process, a Markov chain Monte Carlo algorithm is implemented sequentially to take samples for the model parameters firstly in each iterative step; secondly, IIRS technique is utilized to calculate M_R and K_R , and then take samples for the prediction error variance parameter of σ^2 . Finally, the posterior distributions of the uncertainty parameters are updated based on Bayesian model updating. In addition, the updated modal shape vectors are expanded using modal shape expansion technique, which typically extends the measured mode shape to the unmeasured position. Since mode shape expansion is basically the reverse of model reduction in essence, the same transformation matrix that was utilized for model reduction in Section 4.2 can also be used for modal shape expansion of the identified mode shape vectors of measured DOFs. As a consequence, maximum a posteriori estimation of the identified first two mode shapes for both longitude (EW) and transverse (NS) directions is illustrated in Figure 10.

To further investigate serviceability of the passively-controlled steel building during an earthquake, probabilistic model updating is implemented to estimate the model parameters and infer the response of the structure. Noteworthy that the peak acceleration response of the building for each floor occurs almost at the same time which is the instant of the maximum excitation, thus a segment of time which includes the maximum response in each direction is used to update the dynamic model of the passively-controlled eight-story steel building from the records for analysis. In the end, the updated model parameters can be used for predicting the probabilistic distribution of the structural response. Besides, the maximum a posteriori (MAP) estimates of the response acceleration and interstory drift predictions are depicted in Figures 11 and 12.

The updated model and prediction of the structural response can then be assessed qualitatively and quantitatively. In quantitative senses, the model prediction errors or deviations can be measured by normalized root mean square (NRMS) error, which include the inherent modeling errors and the measurement noise in recorded data. The normalized root mean square used here is defined as follows:

$$\text{NRMS} = \frac{\|y - \hat{y}\|}{\|y\|}, \quad (28)$$

As shown from equation (19), Gaussian likelihood is used to describe the difference between the response of the model and the corresponding measurement. Thus, the detailed likelihood function can be expressed as

where y is the measurement of the response and \hat{y} denotes the corresponding model prediction of structural response. Table 3 lists all the NRMS errors in structural response predictions of updated models under strong earthquakes for 4th floor acceleration, 8th floor acceleration, and 8th interstory drift.

From Table 3, a few interesting observations can be concluded. First, the Bayesian updated models perform a good prediction of the structural behavior with consistently lower NRMS error for various excitations with time histories including different spectral characteristics. Second, the structural responses of transverse (NS) direction possess better estimates and predictions, while the estimates and predicts for longitude (EW) direction fare slightly worse. At last, the updated model predictions actually show a relatively strong qualitative agreement with the corresponding measurement of the response, though the normalized root mean square (NRMS) error greater than 30% generally indicates only a fair prediction. Further, the NRMS errors for acceleration response predicts are no more than 30% except one special case for recording on 7th April 2011, when the passively-controlled steel building just underwent the Great East Japan Earthquake with all dampers on 1st floor completely destroyed and dampers on 3rd and 4th floor with severe oil leakages. The most probable reason for this is that the building produced the largest acceleration response and elicited nonlinear responses under intense earthquake, as passively-controlled devices were barely able to work effectively due to the damage.

For the purpose of exploring the validity of the model shape expansion and the structural response predictions, interstory drifts of 8th floor were compared to the corresponding measurements and are illustrated in Figures 11 and 12 and Table 3. The NRMS errors for predicted interstory drift are significantly larger than that for predicted acceleration response, especially for the longitude (EW) direction. This is partially because that the interstory drift is the relative translational displacement between two consecutive floors, which is generally calculated by the 8th floor displacement subtracting displacement of the 7th floor in this case. Nevertheless, the 7th floor displacement could not be directly identified due to no sensors placed on 7th floor and hence was estimated according to the expended modal shape. Thus, the predicted accuracy of interstory drift is also affected by modal shape expansion method.

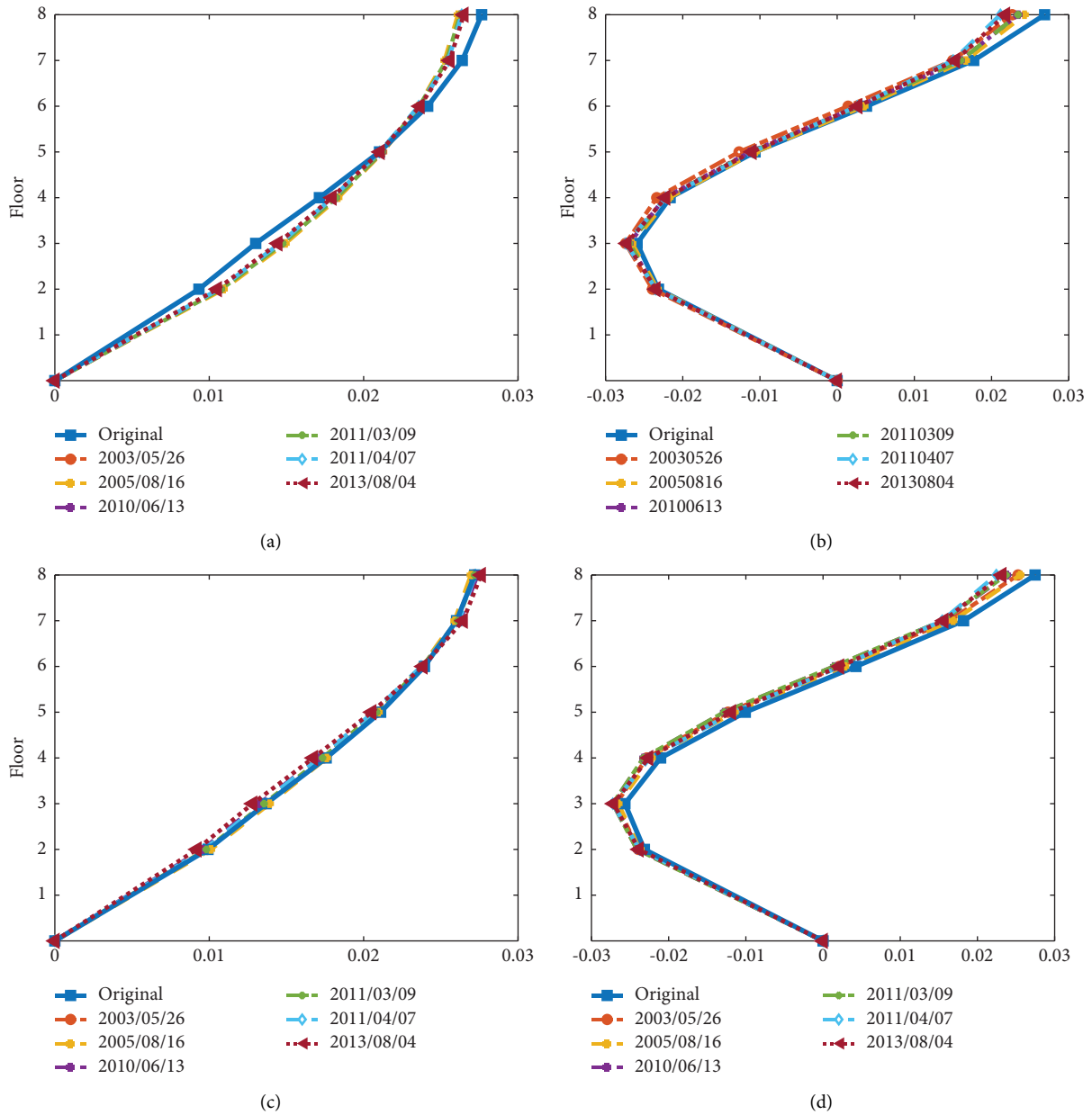


FIGURE 10: Maximum a posteriori estimation of first two mode shapes for longitude (EW) and transverse (NS) directions. (a) 1st mode shape (EW). (b) 2nd mode shape (EW). (c) 1st mode shape (NS). (d) 2nd mode shape (NS).

In the end, the developed probabilistic model updating was able to predict the structural responses using incomplete data, and the predictive performance of this building under strong earthquake could be demonstrated in Figures 11 and 12. Furthermore, high nonlinearity response did not compromise the ability of structural response predictions of the

building. Eventually, it is clear that the updated models are able to seize the dominant dynamic characteristics of the structural behavior both in terms of amplitude and frequency, although there still exist significant discrepancies between the model-predicted and measured responses as shown in Figures 11 and 12 and Table 3.

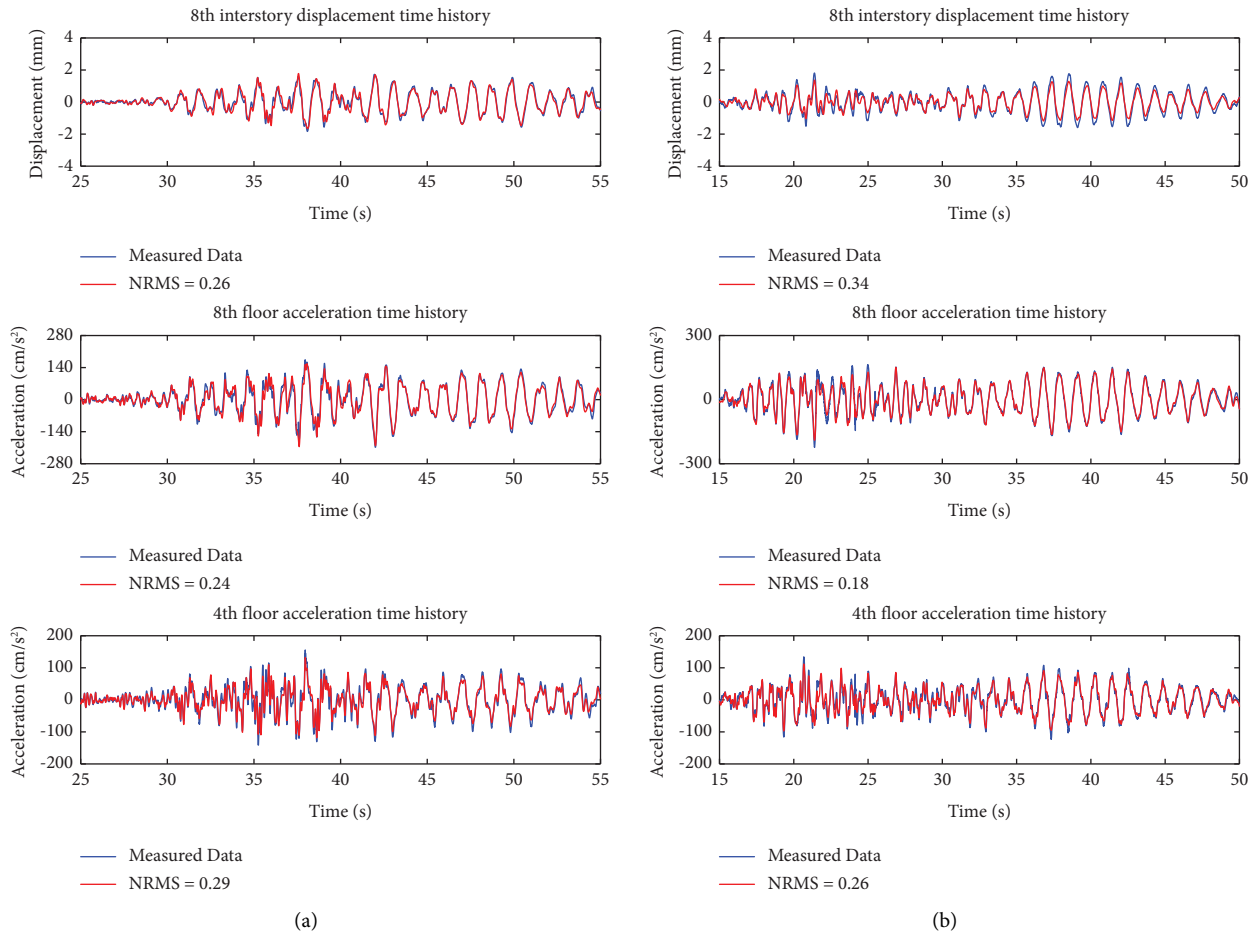
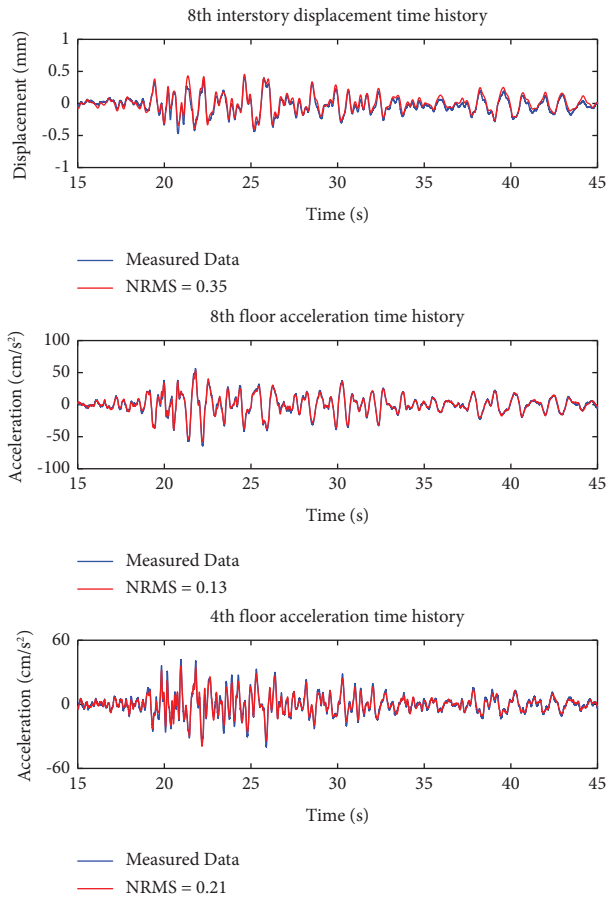
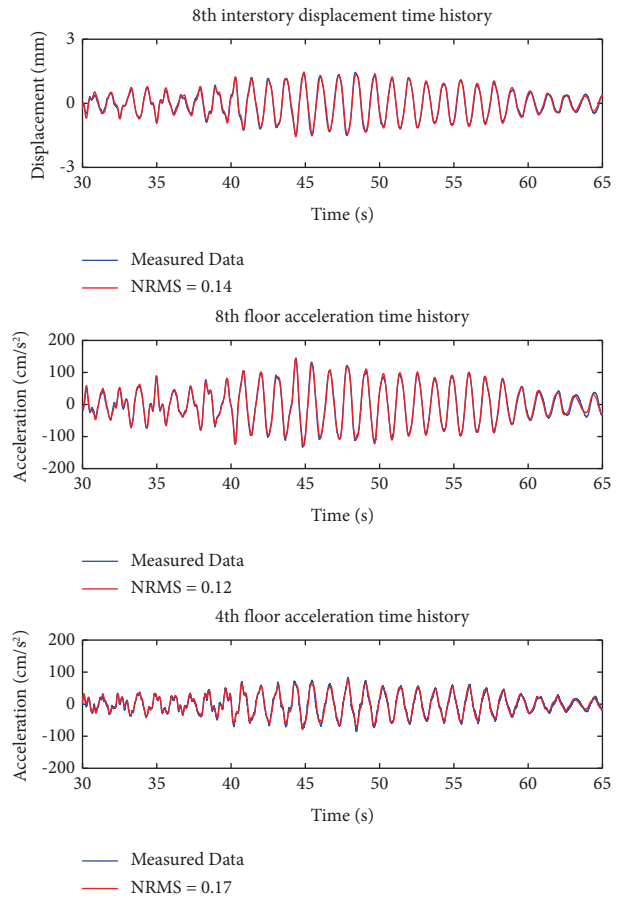


FIGURE 11: Continued.



(c)



(d)

FIGURE 11: Continued.

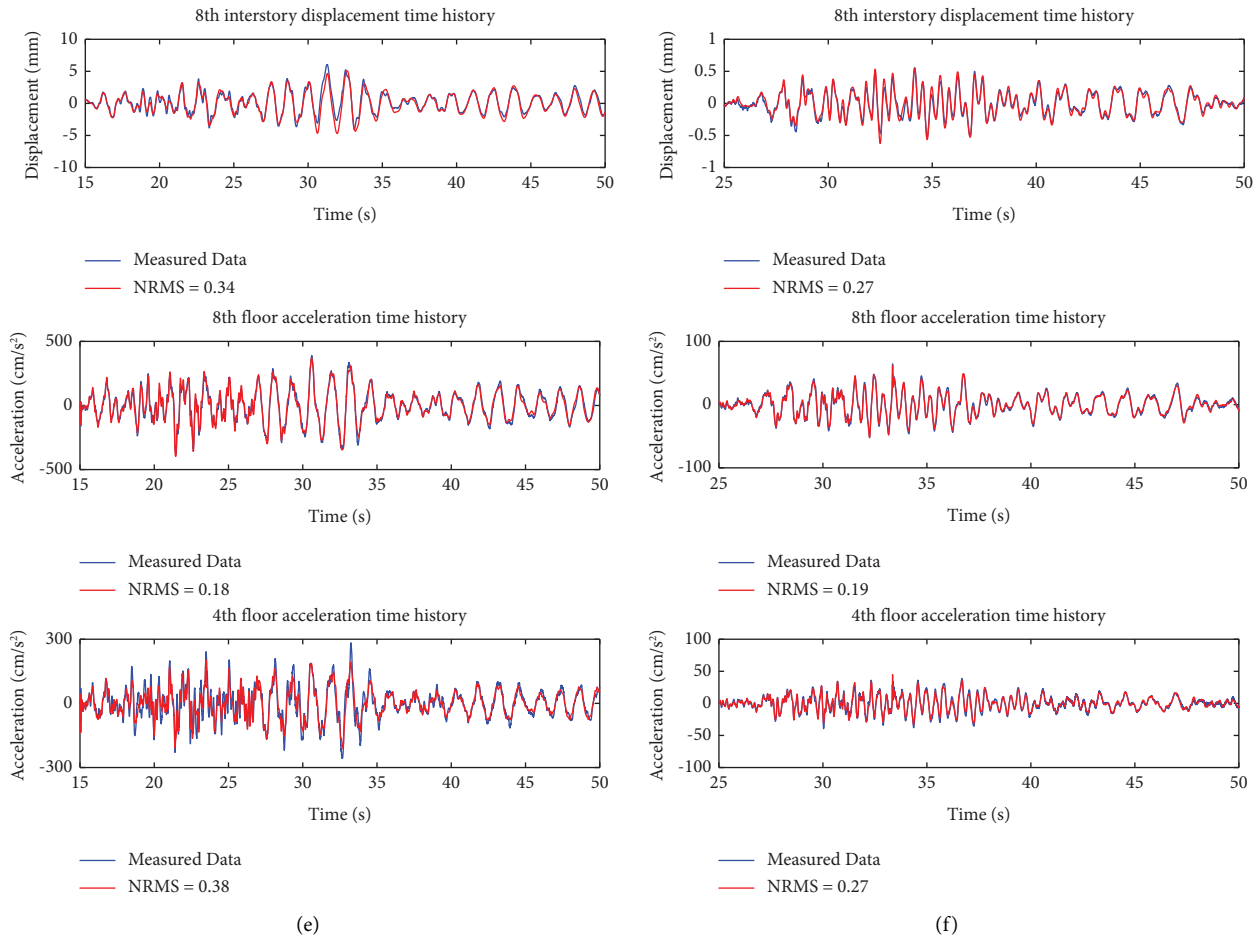


FIGURE 11: Maximum a posteriori estimation of the response acceleration and interstory drift predictions for longitude (EW) direction. (a) Records for 2003/5/26. (b) Records for 2005/08/16. (c) Records for 2010/06/13. (d) Records for 2011/03/09. (e) Records for 2011/04/07. (f) Records for 2013/08/04.

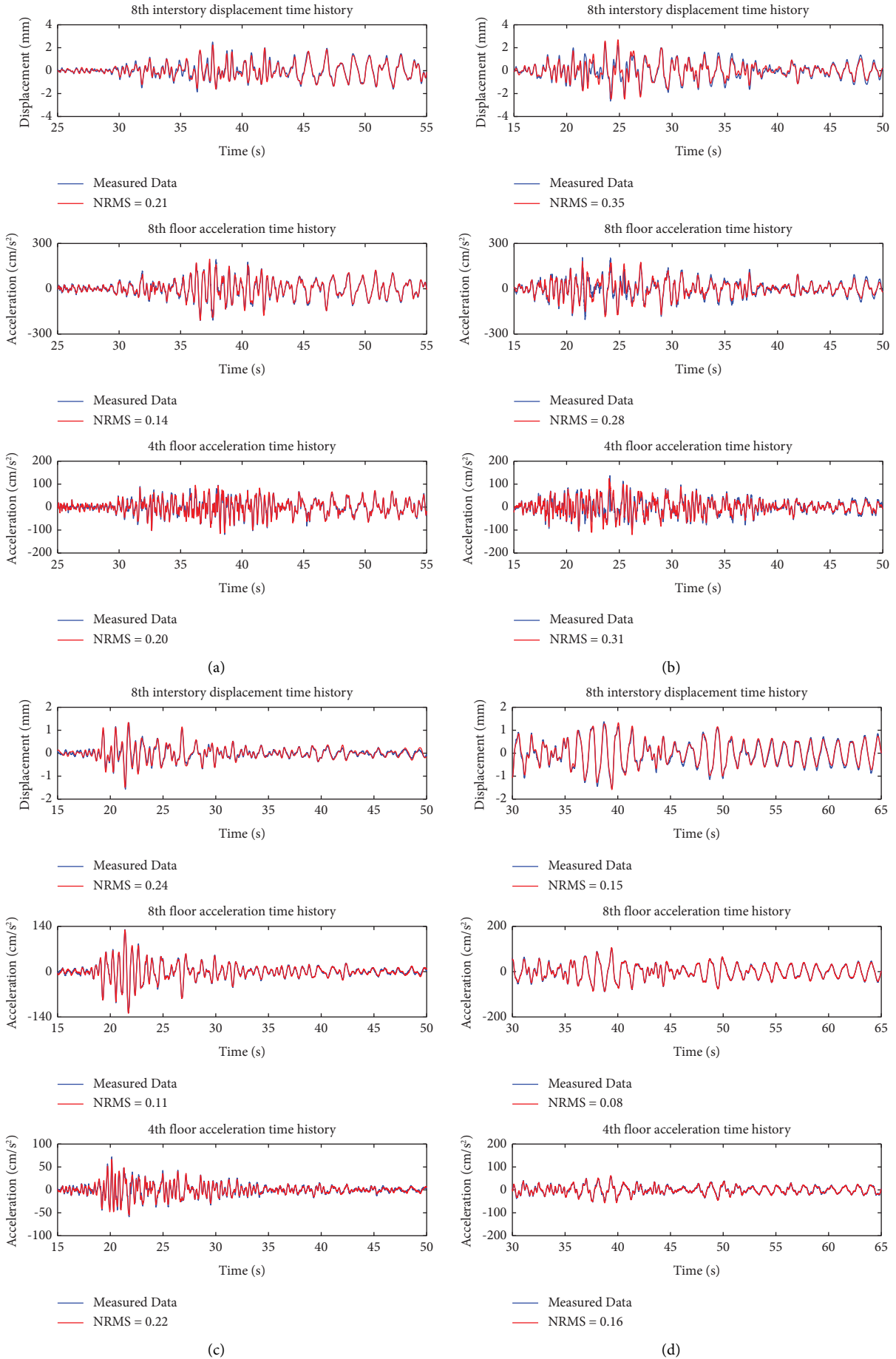


FIGURE 12: Continued.

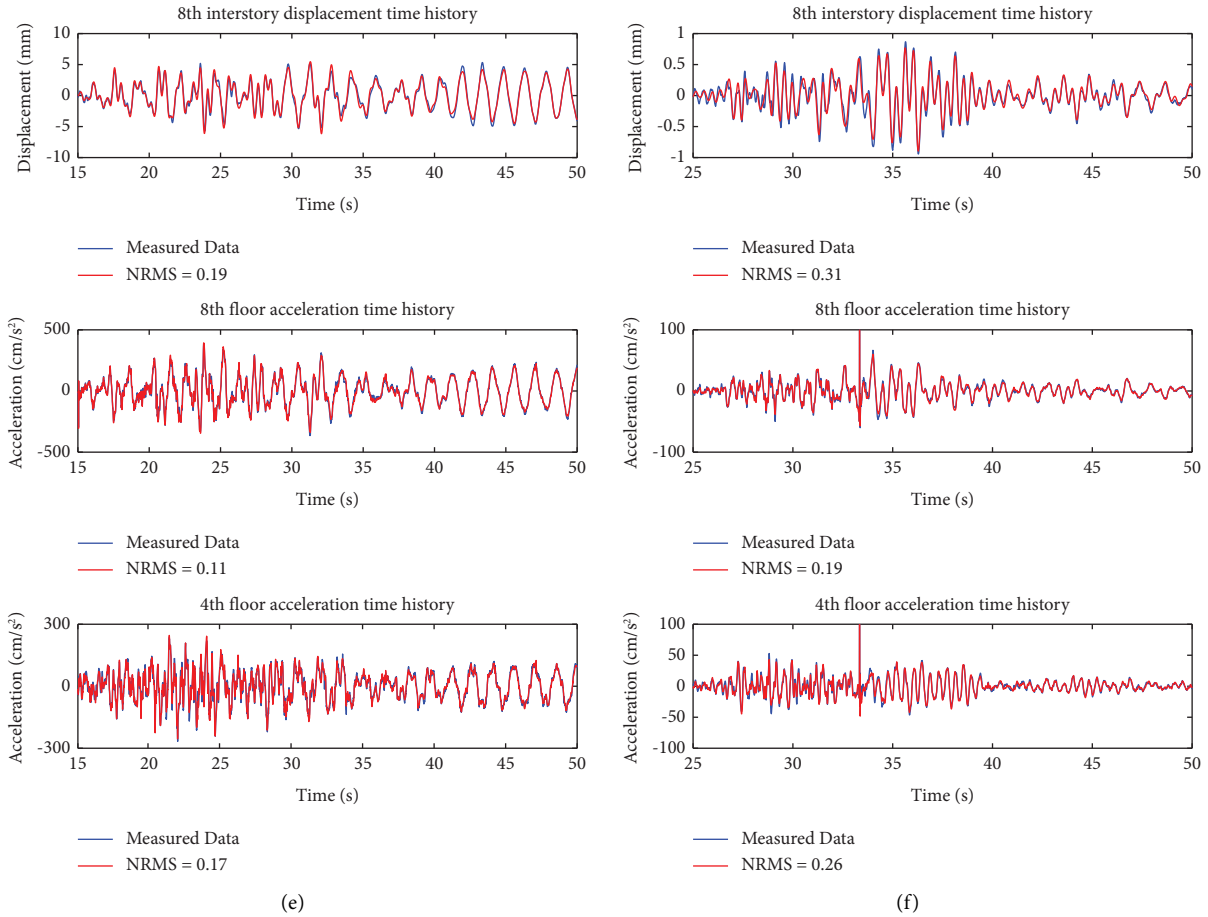


FIGURE 12: Maximum a posteriori estimation of the response acceleration and interstory drift predictions for transverse (NS) direction. (a) Records for 2003/5/26. (b) Records for 2005/08/16. (c) Records for 2010/06/13. (d) Records for 2011/03/09. (e) Records for 2011/04/07. (f) Records for 2013/08/04.

TABLE 3: NRMS errors in structural response predictions of updated models for measured earthquake records.

Date of records (y/m/d)	4 th floor acceleration		8 th floor acceleration		8 th interstory drift	
	EW (%)	NS (%)	EW (%)	NS (%)	EW (%)	NS (%)
2003/5/26	29	20	24	14	26	21
2005/8/16	26	31	18	28	34	35
2010/6/13	21	22	13	11	35	24
2011/3/9	17	16	12	8	14	15
2011/4/7	38	17	18	11	34	19
2013/8/4	27	26	19	19	27	31

5. Summary and Conclusion

In this research, an eight-story passively-controlled steel building with strong motion monitoring system is investigated. Since its construction in 2003, the instrumented steel building has been subjected to approximately 21 earthquakes, four of which were of significant moment magnitude greater than 7.0. In particular, the building survived the 3•11 earthquake without structural damage; however, oil dampers were inspected with varying degrees of damage. Subsequently, the building was retrofitted with tin-rubber bearings. Data-driven stochastic subspace

identification method with a different approach of removing spurious modes is implemented to extract dynamic features of the building from recorded actual earthquake reactions.

Natural frequencies for recording 2003/5/26, 2005/8/16, 2010/6/13, and 2011/3/9, as well as the first two damping ratios, are stable over the eight-year period under study, according to the identified dynamic characteristics of the passively-controlled eight-story steel building. This suggests that the steel building’s overall dynamic properties did not change significantly during this time before the 3•11 earthquake. Nevertheless, for recording 2011/4/7, just after 3•11 earthquake, the identified first two fundamental

frequencies decreased by 12.6% and 11.7% on the average in longitudinal and transverse directions, respectively, which reveals that the oil damper bracing not only gives additional damping but also contributes stiffness to the steel structure. Moreover, due to half of oil dampers lost damping capability, the damping ratios decreased by 35.6% and 40.4% on the average of the first two modes in longitudinal and transverse directions. Additional damping ratio provided by original oil dampers was thus estimated to be around 2%.

Subsequently, the building was retrofitted with tin-rubber bearings replacing the oil dampers in the first floor; after completely repairing, natural frequencies, and damping ratios recovered to a certain level but not as initial. At the same time, the damping ratios increased significantly along with increasing vibration amplitudes. This was mainly attributed to the inelastic response of the tin-rubber bearings. Besides, the observed decreased acceleration magnification ratio (AMR) reflects better seismic resistance performance of the building after retrofitting with tin-rubber bearings. The AMR in vertical direction is distinctly greater than that in horizontal direction. This indicates that the combination of tin-rubber bearings with oil dampers in this building can effectively reduce the acceleration response of the building for horizontal direction rather than vertical direction.

Based on the above system identification and response analysis, probabilistic model updating with a model reduction approach is exploited to estimate the model parameters and infer the structural response using incomplete modal information. The updated models perform a good prediction of the structural behavior with consistently lower NRMS error for different earthquake events. Finally, it is clear that the updated models are able to seize the dominant dynamic characteristics of the structural behavior both in terms of amplitude and frequency, which could be used to infer response of the building for future seismic events and evaluate structural states.

Data Availability

The data used in this study are available on request from the corresponding author.

Disclosure

The findings in this paper are those of the authors and do not necessarily reflect the view of the sponsors.

Conflicts of Interest

The authors declare that they have no conflicts of interest regarding the publication of this paper.

Acknowledgments

The authors express their sincere thanks to the research team who conducted the structural health monitoring of a passively-controlled eight-story steel building with various types of dampers (Leader: Professor Songtao Xue, Tongji

University and Tohoku Institute of Technology). The authors also acknowledge the financial support from the National Key R&D Program of China (Grant nos. 2021YFE0112200 and 2022YFC3801103), the Natural Science Foundation of Shanghai (Grant no. 20ZR1461800); and the Tohoku Institute of Technology research grant.

References

- [1] X. Ji, T. Hikino, K. Kasai, and M. Nakashima, "Damping identification of a full-scale passively controlled five-story steel building structure," *Earthquake Engineering and Structural Dynamics*, vol. 42, no. 2, pp. 277–295, 2013.
- [2] M. C. Constantinou, P. Tsopelas, W. Hammel, and A. N. Sigaher, "Toggle-brace-damper seismic energy dissipation systems," *Journal of Structural Engineering*, vol. 127, no. 2, pp. 105–112, 2001.
- [3] Y. T. Chen and Y. H. Chai, "Seismic design of structures with supplemental Maxwell model-based brace-damper systems," in *World Conference on Earthquake Engineering*, pp. 12–17, Beijing, China, October 2008.
- [4] C. Lee, Y. Chen, L. Chung, and Y. Wang, "Optimal design theories and applications of tuned mass dampers," *Engineering Structures*, vol. 28, no. 1, pp. 43–53, 2006.
- [5] T. T. Soong and B. F. Spencer Jr, "Supplemental energy dissipation: state-of-the-art and state-of-the-practice," *Engineering Structures*, vol. 24, no. 3, pp. 243–259, 2002.
- [6] T. T. Soong and G. F. Dargush, *Passive Energy Dissipation Systems in Structural Engineering*, Wiley, Hoboken, NJ, USA, 1997.
- [7] K. Kasai, A. Mita, H. Kitamura, K. Matsuda, T. A. Morgan, and A. W. Taylor, "Performance of seismic protection technologies during the 2011 Tohoku-Oki earthquake," *Earthquake Spectra*, vol. 29, no. 1_suppl, pp. 265–293, 2013.
- [8] K. Kasai and K. Matsuda, "Full-scale dynamic testing of response-controlled buildings and their components: concepts, methods, and findings," *Earthquake Engineering and Engineering Vibration*, vol. 13, no. S1, pp. 167–181, 2014.
- [9] K. Chang and Y. Lin, "Seismic response of full-scale structure with added viscoelastic dampers," *Journal of Structural Engineering*, vol. 130, no. 4, pp. 600–608, 2004.
- [10] M. L. Lai, K. C. Chang, T. T. Soong, D. S. Hao, and Y. C. Yeh, "Full-scale viscoelastically damped steel frame," *Journal of Structural Engineering*, vol. 121, no. 10, pp. 1443–1447, 1995.
- [11] I. S. Safety, *Recommended Provisions for Seismic Regulations for New Buildings and Other Structures (FEMA 450)*, FEMA, Washington, DC, USA, 2003.
- [12] Y. Minami, S. Yoshitomi, and I. Takewaki, "System identification of super high-rise buildings using limited vibration data during the 2011 Tohoku (Japan) earthquake," *Structural Control and Health Monitoring*, vol. 20, no. 11, pp. 1317–1338, 2013.
- [13] C. Loh, S. Chao, J. Weng, and T. Wu, "Application of subspace identification technique to long-term seismic response monitoring of structures," *Earthquake Engineering and Structural Dynamics*, vol. 44, no. 3, pp. 385–402, 2015.
- [14] D. M. Siringoringo and Y. Fujino, "Seismic response analyses of an asymmetric base-isolated building during the 2011 Great East Japan (Tohoku) Earthquake," *Structural Control and Health Monitoring*, vol. 22, no. 1, pp. 71–90, 2015.
- [15] D. De Domenico, G. Ricciardi, and I. Takewaki, "Design strategies of viscous dampers for seismic protection of

- building structures: a review,” *Soil Dynamics and Earthquake Engineering*, vol. 118, pp. 144–165, 2019.
- [16] I. Takewaki, M. Nakamura, M. Nakamura, and S. Yoshitomi, *System Identification for Structural Health Monitoring*, WIT Press, Billerica, MA, USA, 2012.
- [17] S. F. Ghahari, F. Abazarsa, M. A. Ghannad, and E. Taciroglu, “Response-only modal identification of structures using strong motion data,” *Earthquake Engineering and Structural Dynamics*, vol. 42, no. 8, pp. 1221–1242, 2013.
- [18] A. L. Hong, R. Betti, and C. Lin, “Identification of dynamic models of a building structure using multiple earthquake records,” *Structural Control and Health Monitoring*, vol. 16, no. 2, pp. 178–199, 2009.
- [19] D. M. Siringoringo and Y. Fujino, “System identification applied to long-span cable-supported bridges using seismic records,” *Earthquake Engineering and Structural Dynamics*, vol. 37, no. 3, pp. 361–386, 2008.
- [20] C. Rainieri and G. Fabbrocino, *Operational Modal Analysis of Civil Engineering Structures*, Springer, Berlin, Germany, 2014.
- [21] T. Katayama, *Subspace Methods for System Identification*, Springer, Berlin, Germany, 2005.
- [22] P. Van Overschee and B. L. De Moor, *Subspace Identification for Linear Systems: Theory—Implementation—Applications*, Springer Science and Business Media, Berlin, Germany, 2012.
- [23] E. Reynders, R. Pintelon, and G. De Roeck, “Uncertainty bounds on modal parameters obtained from stochastic subspace identification,” *Mechanical Systems and Signal Processing*, vol. 22, no. 4, pp. 948–969, 2008.
- [24] R. S. Pappa, K. B. Elliott, and A. Schenk, “Consistent-mode indicator for the eigensystem realization algorithm,” *Journal of Guidance, Control, and Dynamics*, vol. 16, no. 5, pp. 852–858, 1993.
- [25] A. Olivier and A. W. Smyth, “Review of nonlinear filtering for SHM with an exploration of novel higher-order Kalman filtering algorithms for uncertainty quantification,” *Journal of Engineering Mechanics*, vol. 143, no. 11, Article ID 4017128, 2017.
- [26] S. Mukhopadhyay, H. Lus, and R. Betti, “Structural identification with incomplete instrumentation and global identifiability requirements under base excitation,” *Structural Control and Health Monitoring*, vol. 22, no. 7, pp. 1024–1047, 2015.
- [27] B. Jaishi and W. Ren, “Structural finite element model updating using ambient vibration test results,” *Journal of Structural Engineering*, vol. 131, no. 4, pp. 617–628, 2005.
- [28] H. F. Lam, H. Y. Peng, and S. K. Au, “Development of a practical algorithm for Bayesian model updating of a coupled slab system utilizing field test data,” *Engineering Structures*, vol. 79, pp. 182–194, 2014.
- [29] B. Goller and G. I. Schuëller, “Investigation of model uncertainties in Bayesian structural model updating,” *Journal of Sound and Vibration*, vol. 330, no. 25, pp. 6122–6136, 2011.
- [30] J. Ching and J. L. Beck, “New Bayesian model updating algorithm applied to a structural health monitoring benchmark,” *Structural Health Monitoring*, vol. 3, no. 4, pp. 313–332, 2004.
- [31] S. Monchetti, C. Viscardi, M. Betti, and G. Bartoli, “Bayesian-based model updating using natural frequency data for historic masonry towers,” *Probabilistic Engineering Mechanics*, vol. 70, Article ID 103337, 2022.
- [32] E. Asgariéh, B. Moaveni, A. R. Barbosa, and E. Chatzi, “Nonlinear model calibration of a shear wall building using time and frequency data features,” *Mechanical Systems and Signal Processing*, vol. 85, pp. 236–251, 2017.
- [33] I. Behmanesh and B. Moaveni, “Probabilistic identification of simulated damage on the Dowling Hall footbridge through Bayesian finite element model updating,” *Structural Control and Health Monitoring*, vol. 22, no. 3, pp. 463–483, 2015.
- [34] X. Zhou, C. Kim, F. Zhang, and K. Chang, “Vibration-based Bayesian model updating of an actual steel truss bridge subjected to incremental damage,” *Engineering Structures*, vol. 260, Article ID 114226, 2022.
- [35] Y. Xin, H. Hao, J. Li, Z. Wang, H. Wan, and W. Ren, “Bayesian based nonlinear model updating using instantaneous characteristics of structural dynamic responses,” *Engineering Structures*, vol. 183, pp. 459–474, 2019.
- [36] H. F. Lam, J. H. Yang, and S. K. Au, “Markov chain Monte Carlo-based Bayesian method for structural model updating and damage detection,” *Structural Control and Health Monitoring*, vol. 25, no. 4, 2018.
- [37] P. Baraldi, F. Mangili, and E. Zio, “Investigation of uncertainty treatment capability of model-based and data-driven prognostic methods using simulated data,” *Reliability Engineering and System Safety*, vol. 112, pp. 94–108, 2013.
- [38] A. Gelman, W. R. Gilks, and G. O. Roberts, “Weak convergence and optimal scaling of random walk Metropolis algorithms,” *Annals of Applied Probability*, vol. 7, no. 1, pp. 110–120, 1997.
- [39] A. Batou, C. Soize, and S. Audebert, “Model identification in computational stochastic dynamics using experimental modal data,” *Mechanical Systems and Signal Processing*, vol. 50–51, pp. 307–322, 2015.
- [40] W. Yan and L. S. Katafygiotis, “A novel Bayesian approach for structural model updating utilizing statistical modal information from multiple setups,” *Structural Safety*, vol. 52, pp. 260–271, 2015.
- [41] J. Ching, M. Muto, and J. L. Beck, “Structural model updating and health monitoring with incomplete modal data using Gibbs sampler,” *Computer-Aided Civil and Infrastructure Engineering*, vol. 21, no. 4, pp. 242–257, 2006.
- [42] K. V. Yuen, J. L. Beck, and L. S. Katafygiotis, “Efficient model updating and health monitoring methodology using incomplete modal data without mode matching,” *Structural Control and Health Monitoring*, vol. 13, no. 1, pp. 91–107, 2006.
- [43] J. L. Beck, S. K. Au, and M. W. Vanik, “Monitoring structural health using a probabilistic measure,” *Computer-Aided Civil and Infrastructure Engineering*, vol. 16, no. 1, pp. 1–11, 2001.
- [44] L. Xie, M. Cao, N. Funaki, H. Tang, and S. Xue, “Performance study of an eight-story steel building equipped with oil dampers damaged during the 2011 Great East Japan earthquake Part 1: structural identification and damage reasoning,” *Journal of Asian Architecture and Building Engineering*, vol. 14, no. 1, pp. 181–188, 2015.
- [45] Y. Tong, S. Xue, L. Xie, and H. Tang, “Damping evaluation of an eight-story steel building with nonlinear oil damper under strong earthquakes,” *Journal of Building Engineering*, vol. 67, Article ID 106004, 2023.
- [46] M. Cao, L. Xie, H. Tang, N. Funaki, and S. Xue, “Performance study of an 8-story steel building equipped with oil damper

- damaged during the 2011 great east Japan earthquakepart 2: novel retrofit strategy,” *Journal of Asian Architecture and Building Engineering*, vol. 15, no. 2, pp. 303–310, 2018.
- [47] H. S. Ulusoy, M. Q. Feng, and P. J. Fanning, “System identification of a building from multiple seismic records,” *Earthquake Engineering and Structural Dynamics*, vol. 40, no. 6, pp. 661–674, 2011.
- [48] J. L. Beck and P. C. Jennings, “Structural identification using linear models and earthquake records,” *Earthquake Engineering and Structural Dynamics*, vol. 8, no. 2, pp. 145–160, 1980.
- [49] R. Ghanem and M. Shinozuka, “Structural-system identification. I: theory,” *Journal of Engineering Mechanics*, vol. 121, no. 2, pp. 255–264, 1995.
- [50] H. F. Lam, J. Hu, and M. O. Adeagbo, “Bayesian model updating of a 20-story office building utilizing operational modal analysis results,” *Advances in Structural Engineering*, vol. 22, no. 16, pp. 3385–3394, 2019.
- [51] M. Aghagholizadeh and F. N. Catbas, *A Review of Model Updating Methods for Civil Infrastructure Systems. Computational Techniques for Civil and Structural Engineering*, Saxe-Coburg Publications, Stirlingshire, 2015.
- [52] S. H. Cheung and J. L. Beck, “Bayesian model updating using hybrid Monte Carlo simulation with application to structural dynamic models with many uncertain parameters,” *Journal of Engineering Mechanics*, vol. 135, no. 4, pp. 243–255, 2009.
- [53] H. Sun and O. Büyüköztürk, “Probabilistic updating of building models using incomplete modal data,” *Mechanical Systems and Signal Processing*, vol. 75, pp. 27–40, 2016.
- [54] M. Friswell and J. E. Mottershead, *Finite Element Model Updating in Structural Dynamics*, Springer Science and Business Media, Berlin, Germany, 2013.
- [55] Y. Tong, L. Xie, S. Xue, and H. Tang, “Identification of a monitoring nonlinear oil damper using particle filtering approach,” *Mechanical Systems and Signal Processing*, vol. 189, Article ID 110020, 2023.